Supplemental Data

A

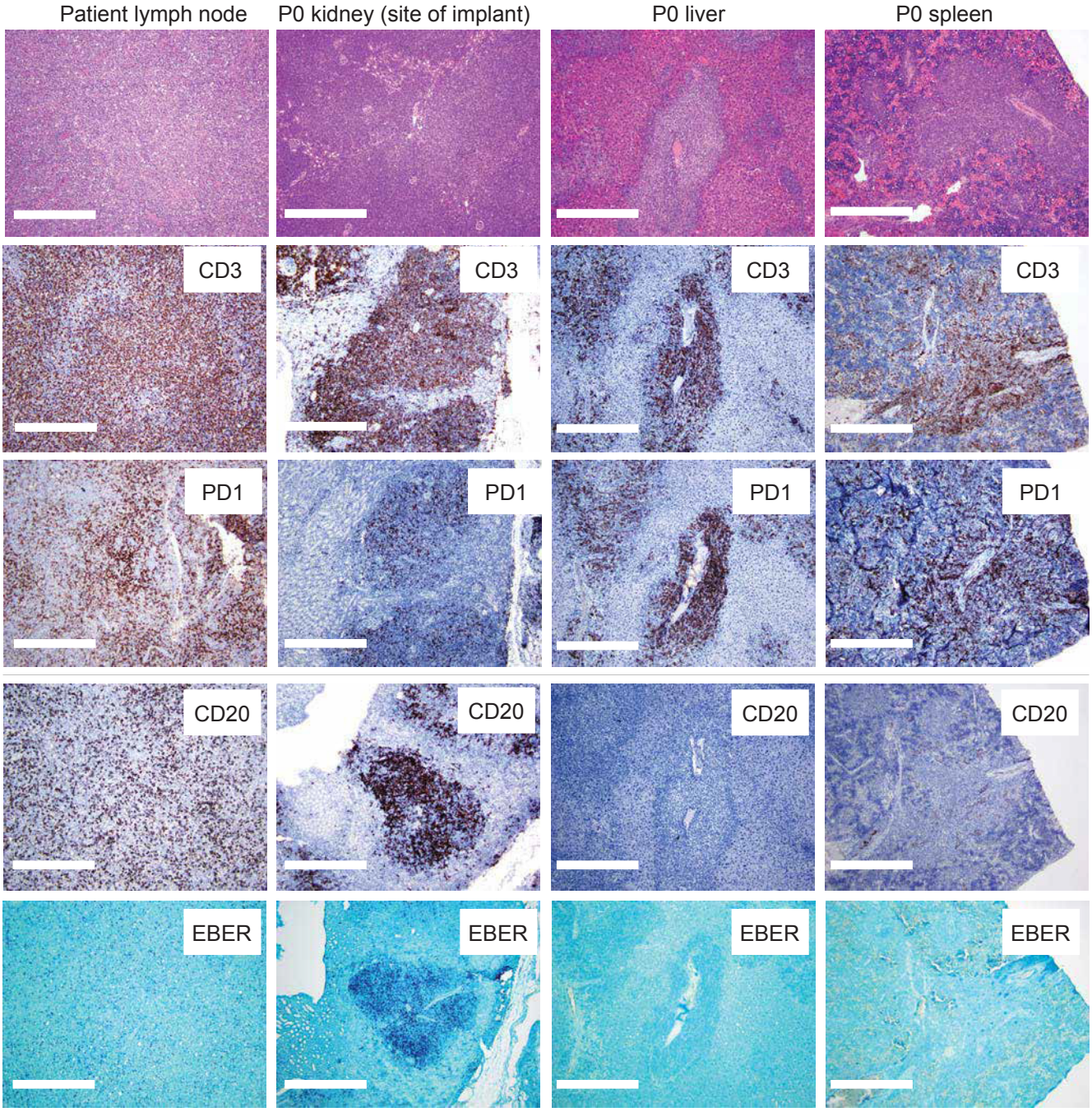

B

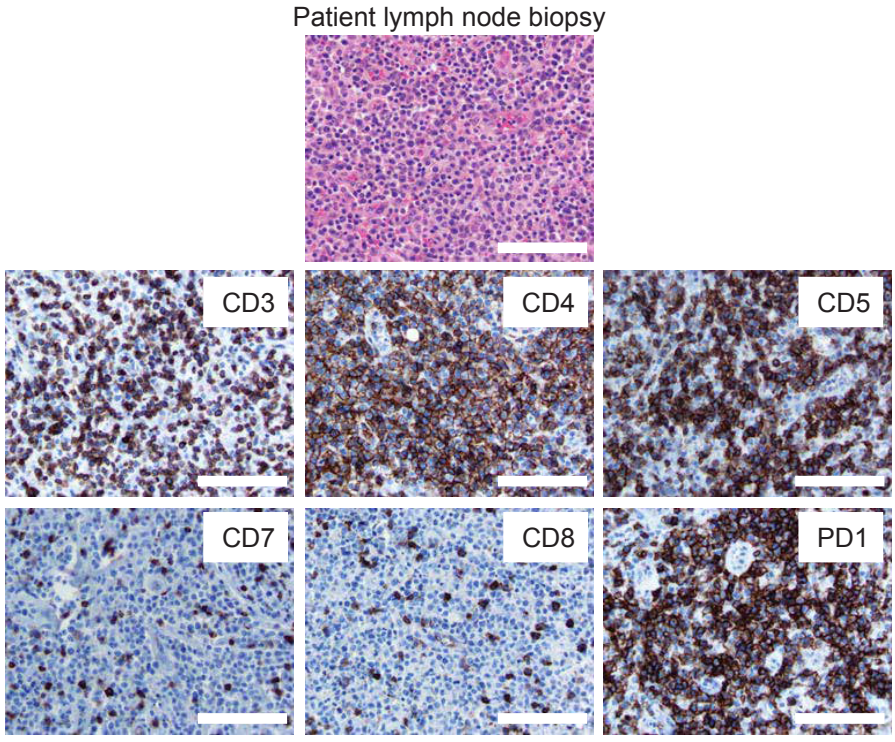
Patient lymph node biopsy
CD3
CD4
CD5
CD7
CD8
PD1

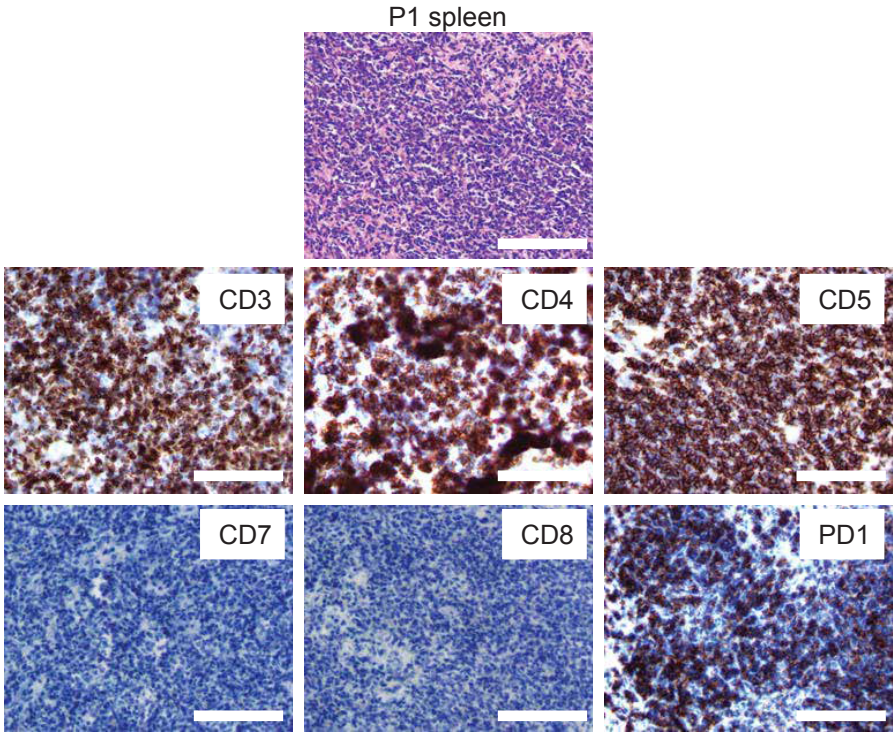
P1 spleen
CD3
CD4
CD5
CD7
CD8
PD1

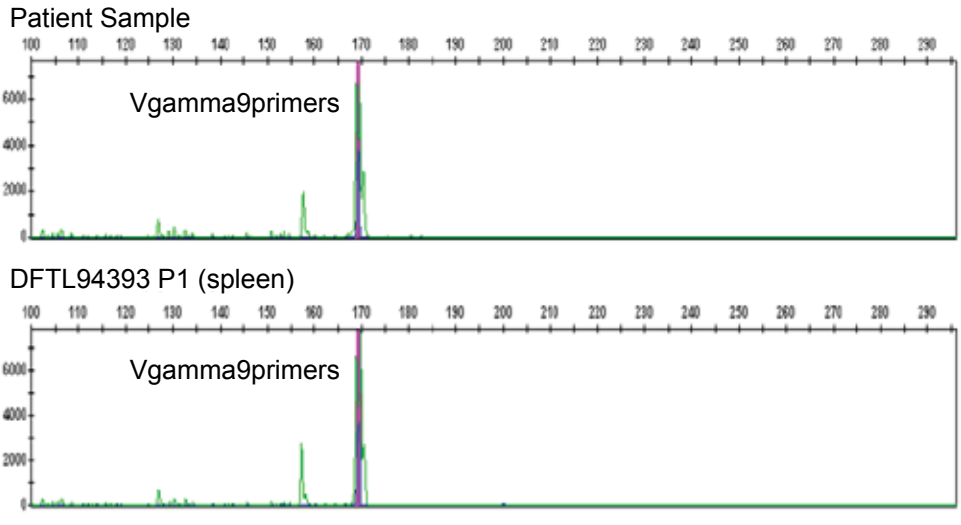
Patient Sample
Vgamma9primers
DFTL94393 P1 (spleen)
Vgamma9primers

C

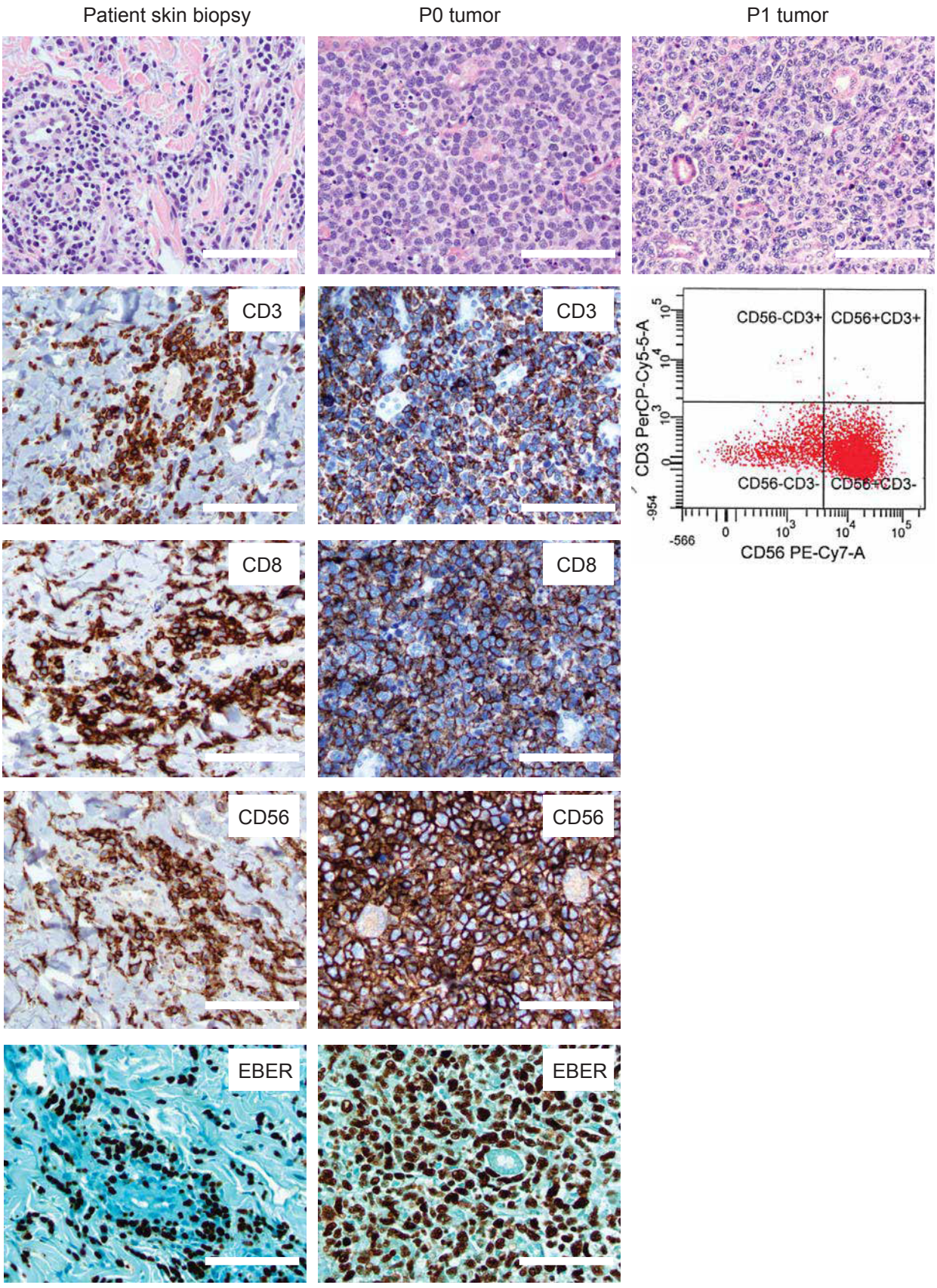
Patient skin biopsy
P0 tumor
P1 tumor
CD3
CD3
CD56-CD3+
CD56+CD3+
CD56-CD3-
CD56+CD3-
CD3 PerCP-Cy5-5-A
CD56 PE-Cy7-A
-954
-566
0
10^3
10^4
10^5
CD8
CD8
CD56
CD56
EBER
EBER

D

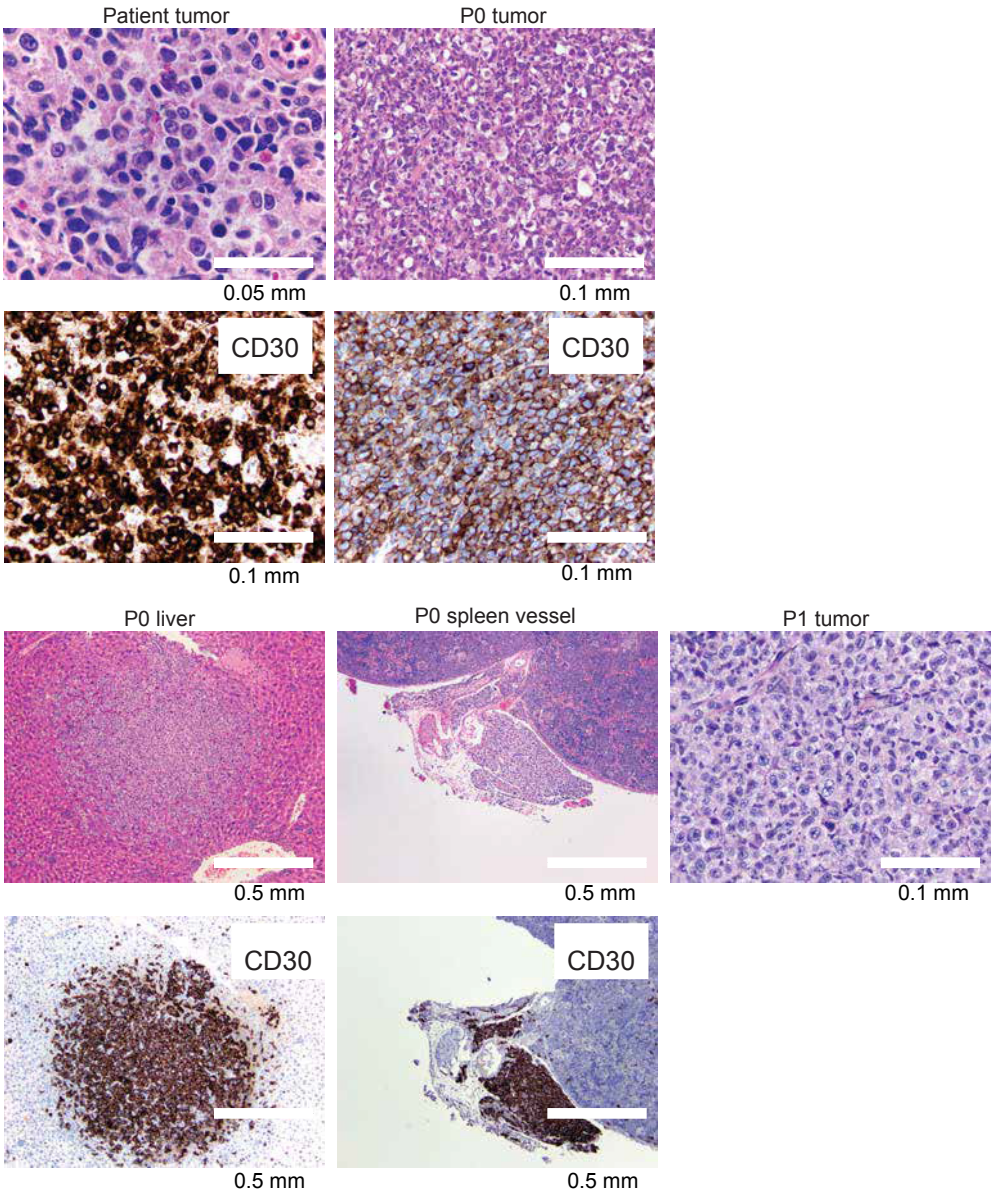
Patient tumor
P0 tumor
0.05 mm
0.1 mm
CD30
CD30
0.1 mm
0.1 mm
P0 liver
P0 spleen vessel
P1 tumor
0.5 mm
0.5 mm
0.1 mm
CD30
CD30
0.5 mm
0.5 mm

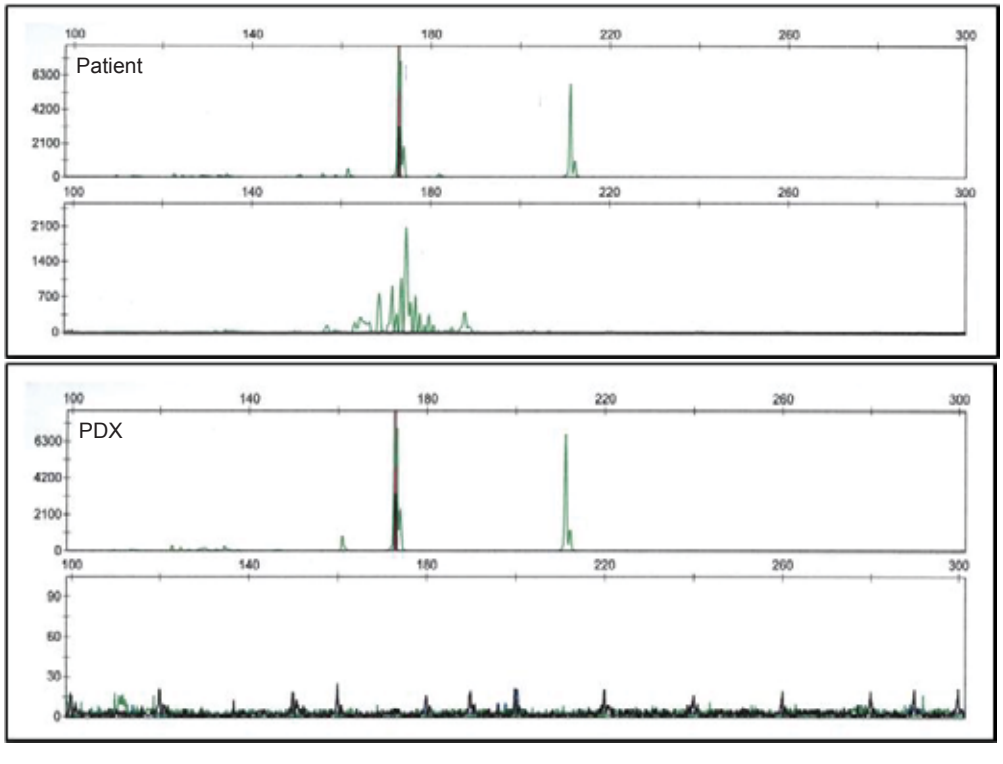
Patient
PDX
100
140
180
220
260
300
6300
4200
2100
0
1400
700
90
60
30

E

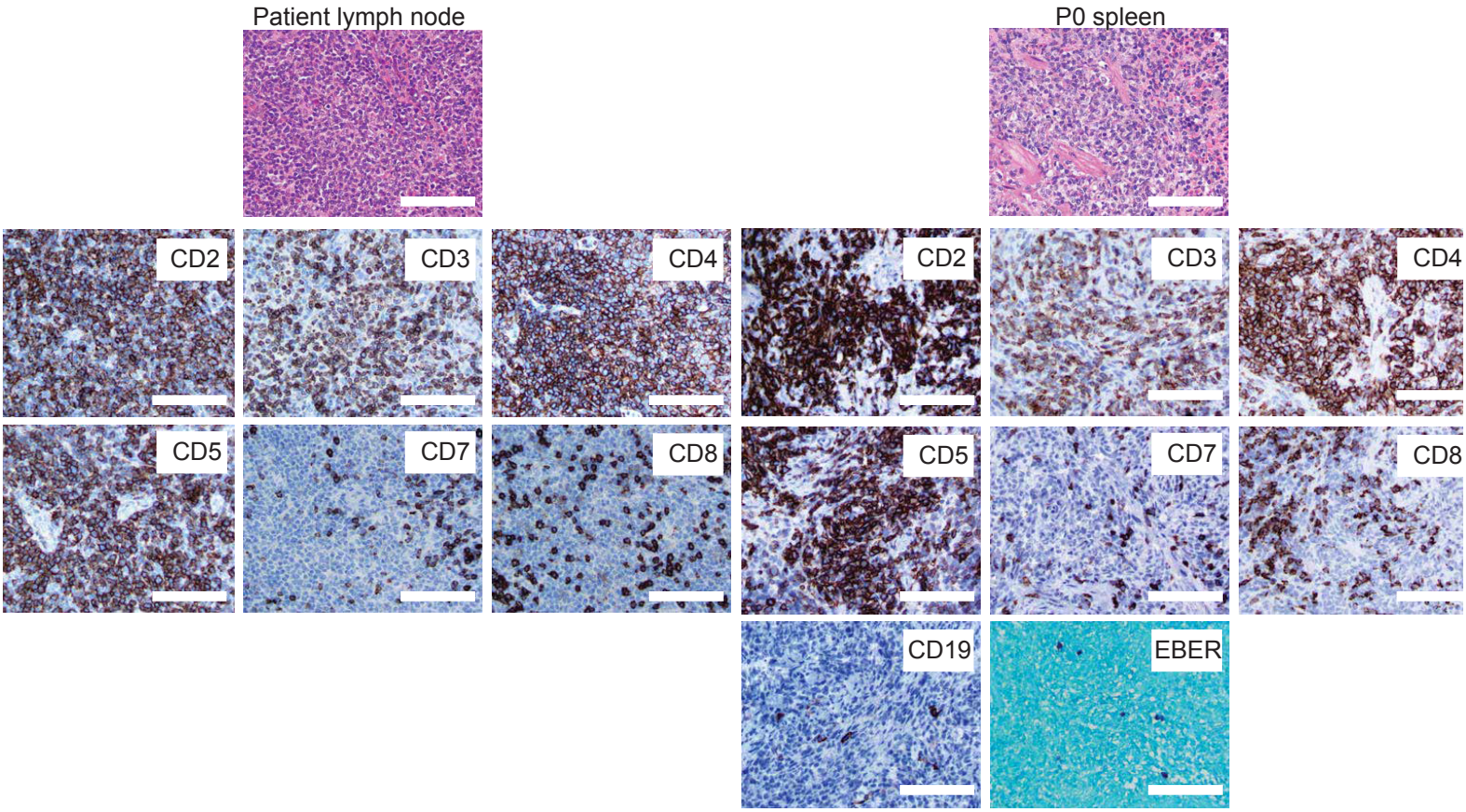
Patient lymph node
P0 spleen
CD2
CD3
CD4
CD2
CD3
CD4
CD5
CD7
CD8
CD5
CD7
CD8
CD19
EBER

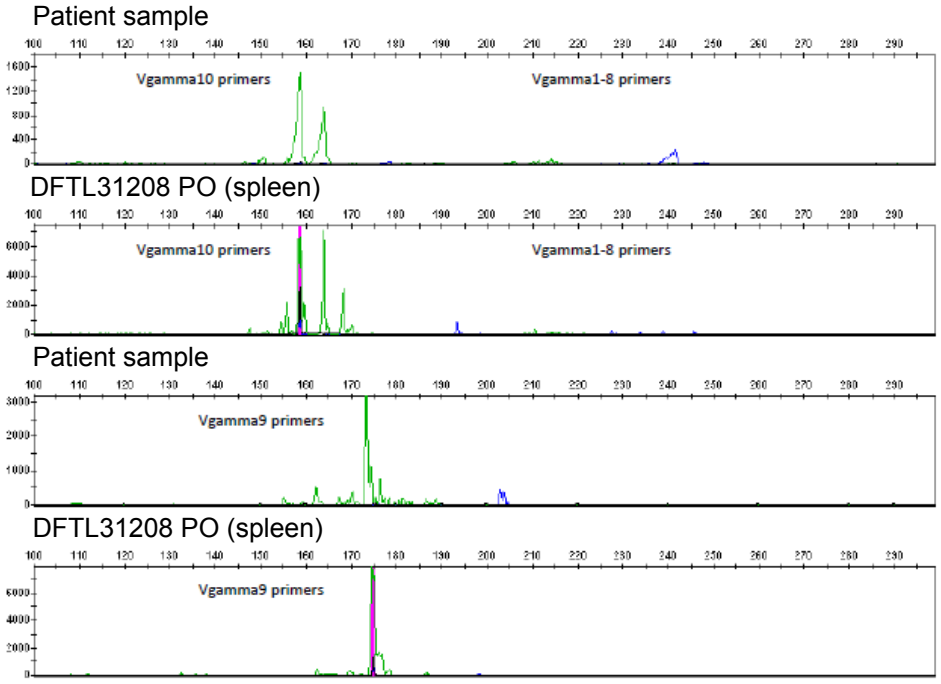
Patient sample
Vgamma10 primers
Vgamma1-8 primers
DFTL31208 PO (spleen)
Vgamma10 primers
Vgamma1-8 primers
Patient sample
Vgamma9 primers
DFTL31208 PO (spleen)
Vgamma9 primers

F

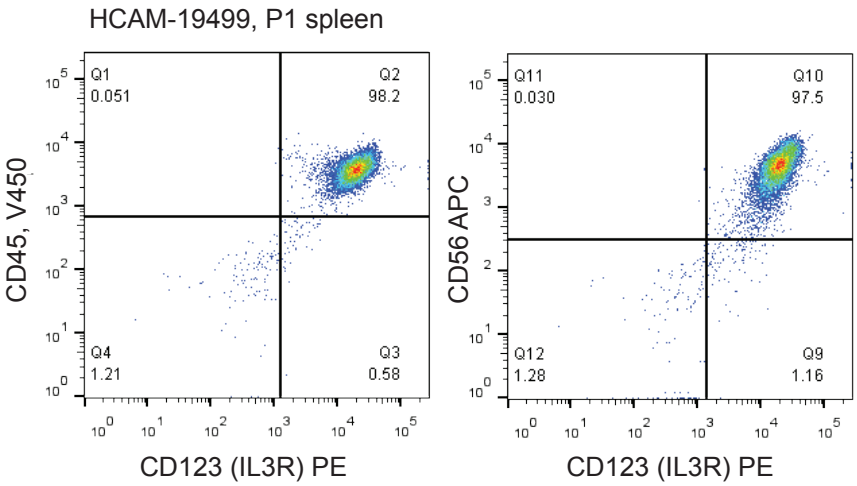
HCAM-19499, P1 spleen
Q1
0.051
Q2
98.2
Q4
1.21
Q3
0.58
CD45, V450
CD123 (IL3R) PE
Q11
0.030
Q10
97.5
Q12
1.28
Q9
1.16
CD56 APC
CD123 (IL3R) PE

G

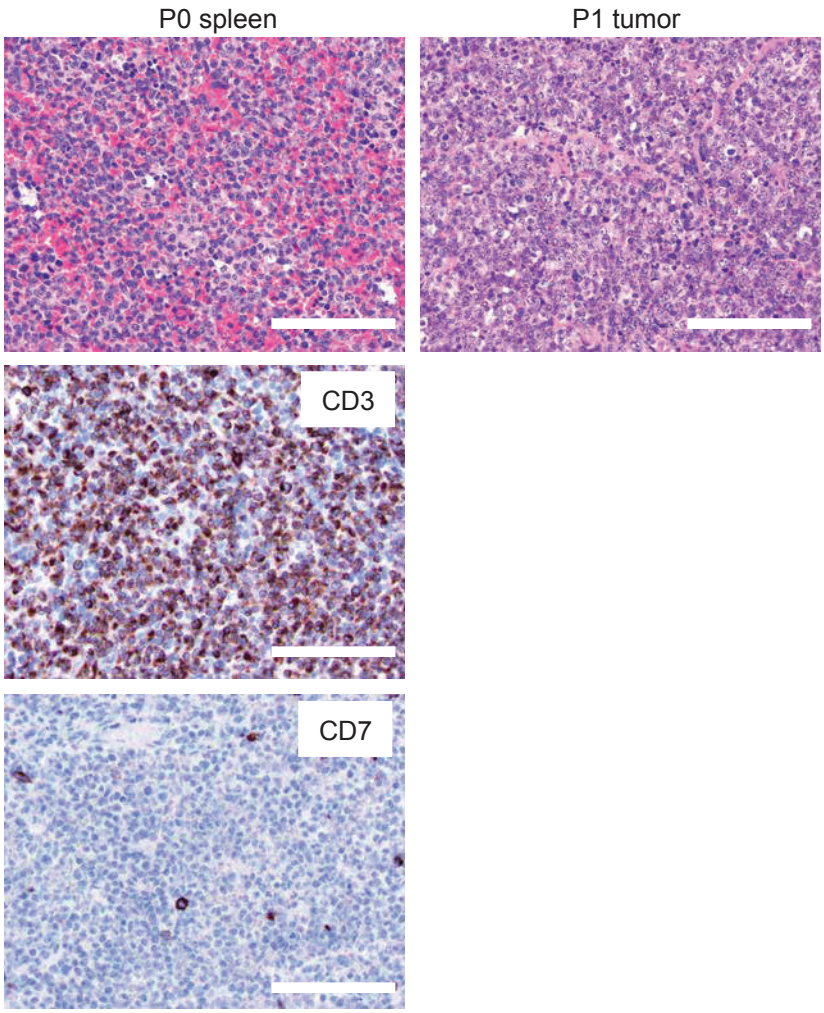
P0 spleen
P1 tumor
CD3
CD7

H

Patient skin

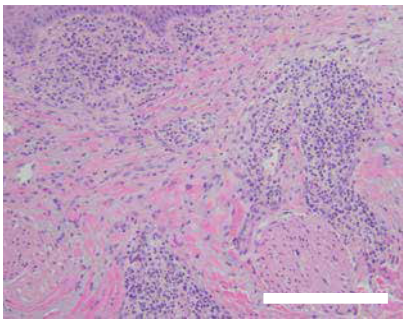

0.5 mm

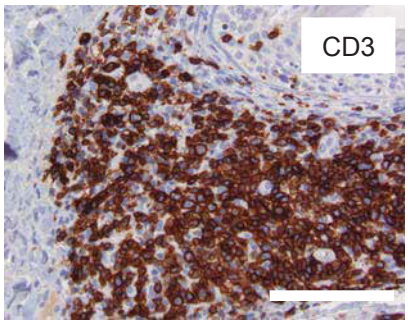

0.1 mm

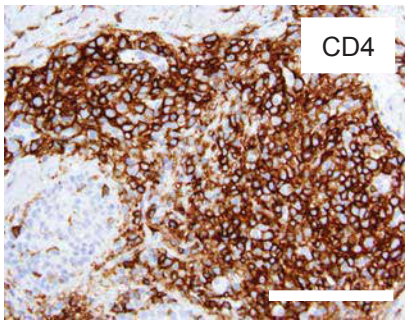

0.1 mm

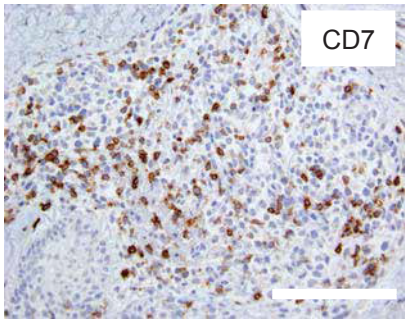

0.1 mm

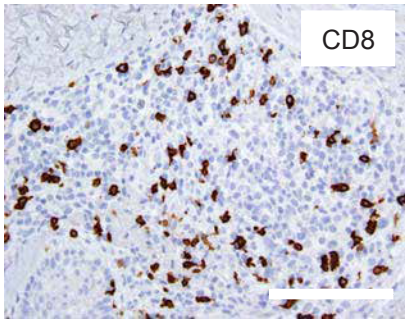

0.1 mm

P1 skin

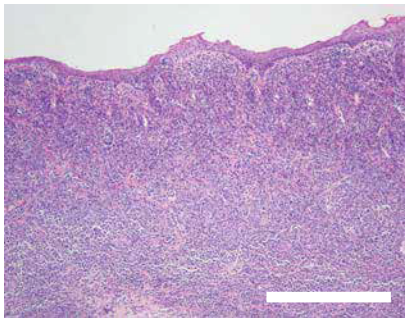

0.5 mm

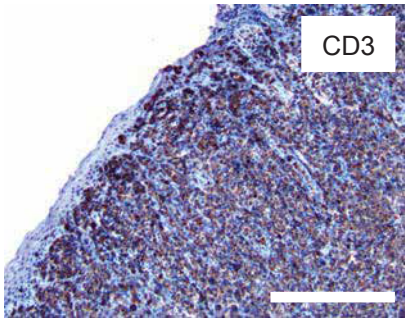

0.25 mm

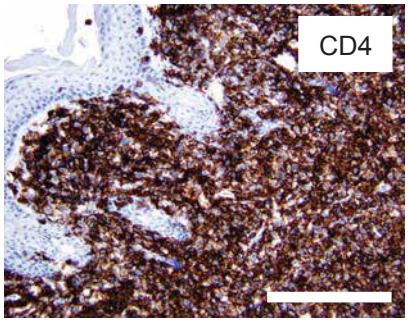

0.25 mm

P1 spleen

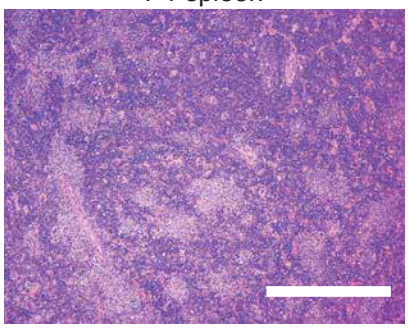

0.5 mm

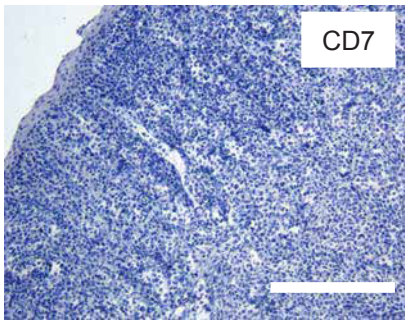

0.25 mm

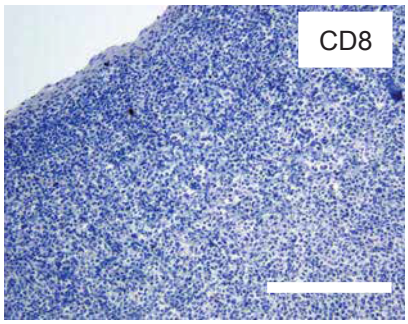

0.25 mm

I

Patient lymph node

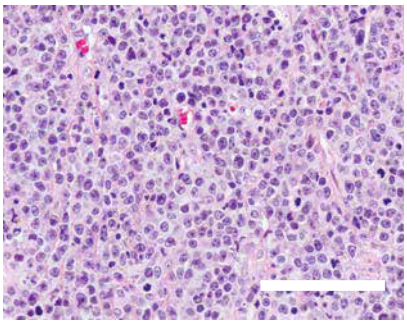

0.1 mm

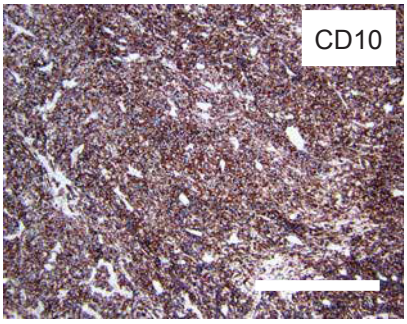

0.5 mm

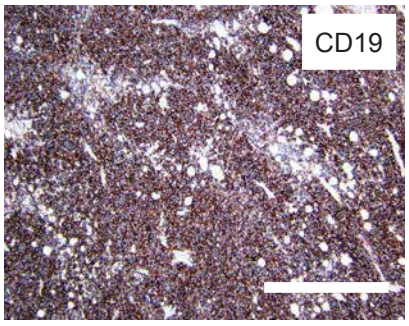

0.5 mm

P0 tumor

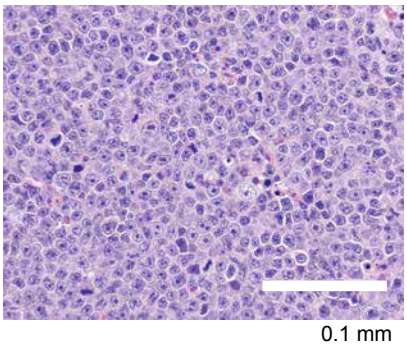

0.1 mm

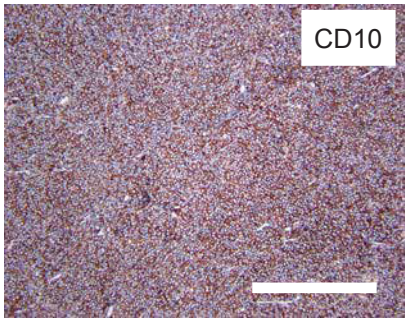

0.5 mm

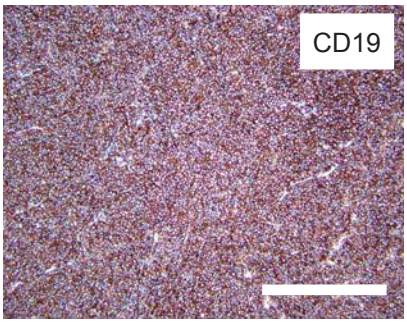

0.5 mm

P1 tumor

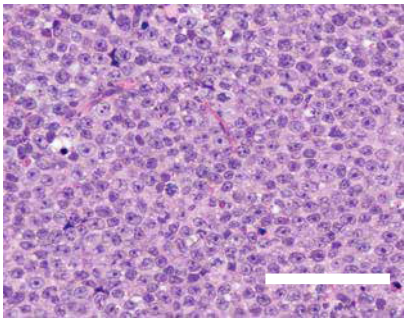

0.1 mm

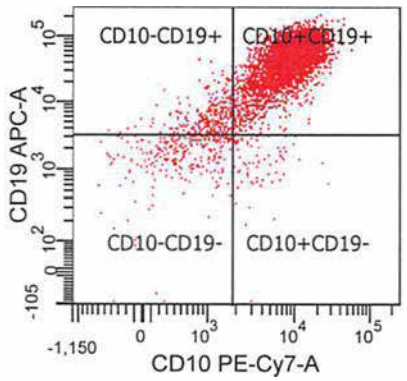

P2 brain

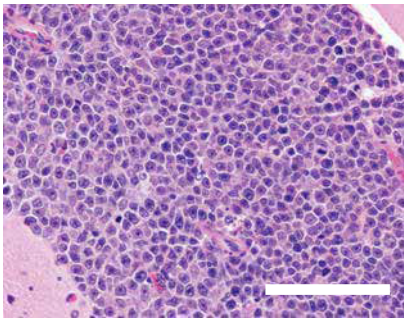

0.1 mm

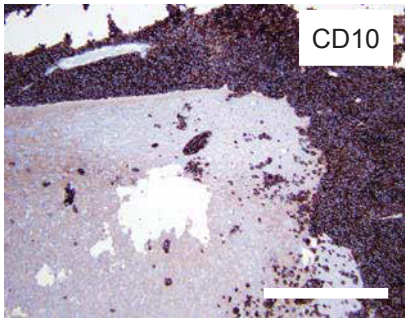

0.5 mm

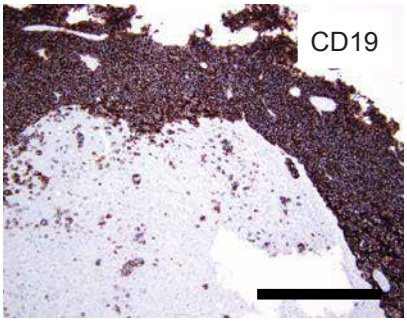

0.5 mm

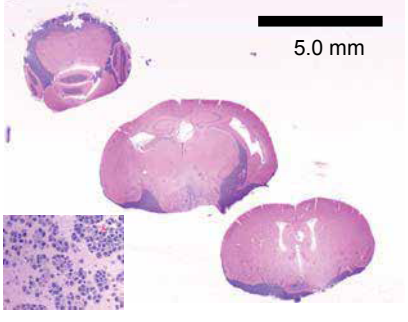

J

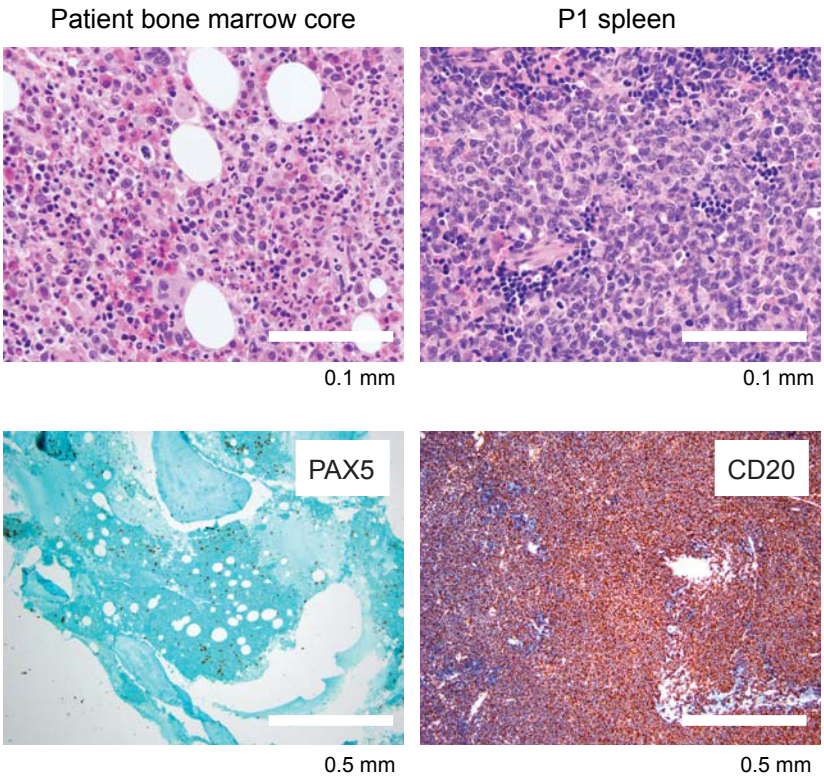
Patient bone marrow core
P1 spleen
0.1 mm
0.1 mm
PAX5
CD20
0.5 mm
0.5 mm

K

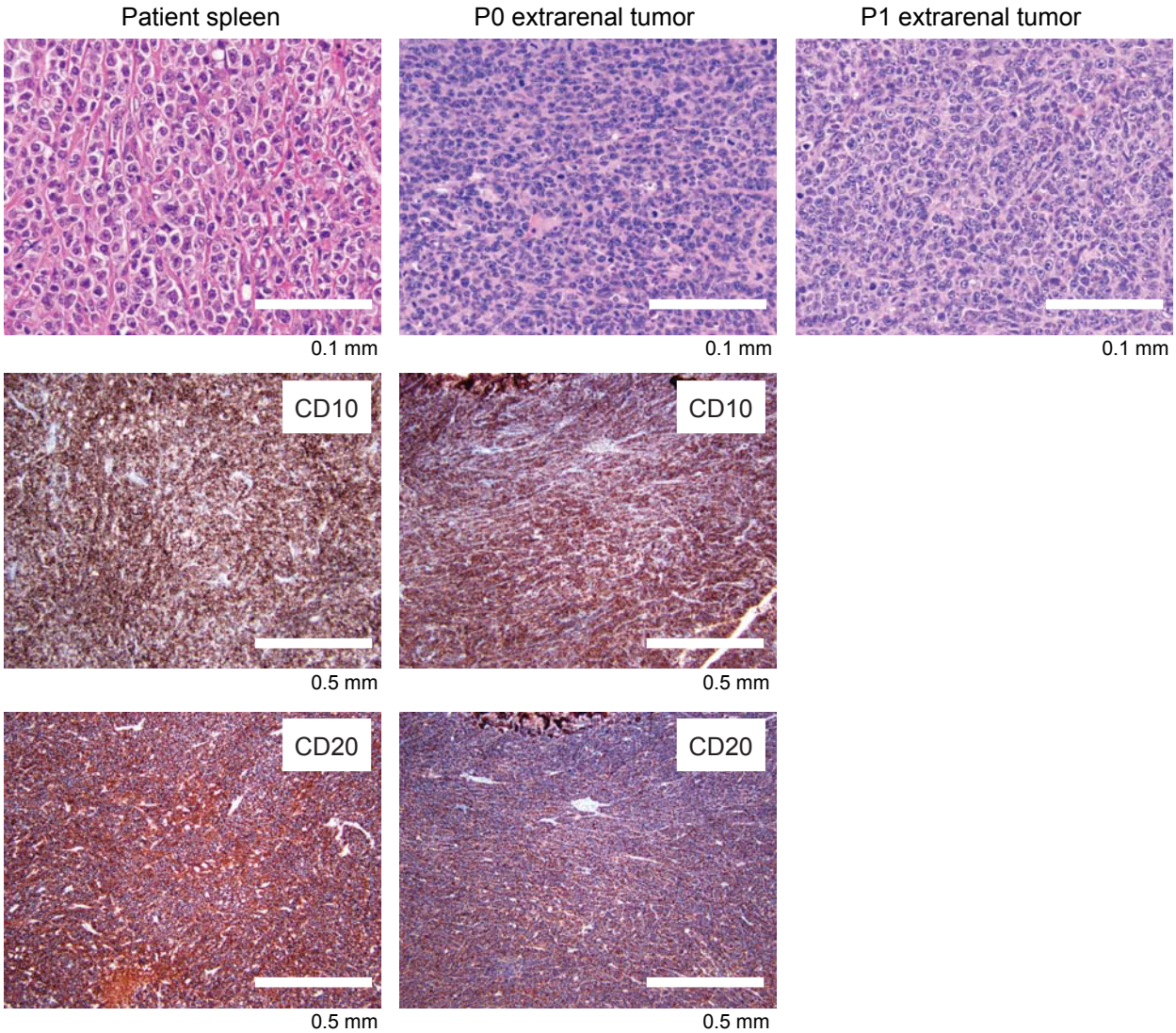
Patient spleen
P0 extrarenal tumor
P1 extrarenal tumor
0.1 mm
0.1 mm
0.1 mm
CD10
CD10
0.5 mm
0.5 mm
CD20
CD20
0.5 mm
0.5 mm

L

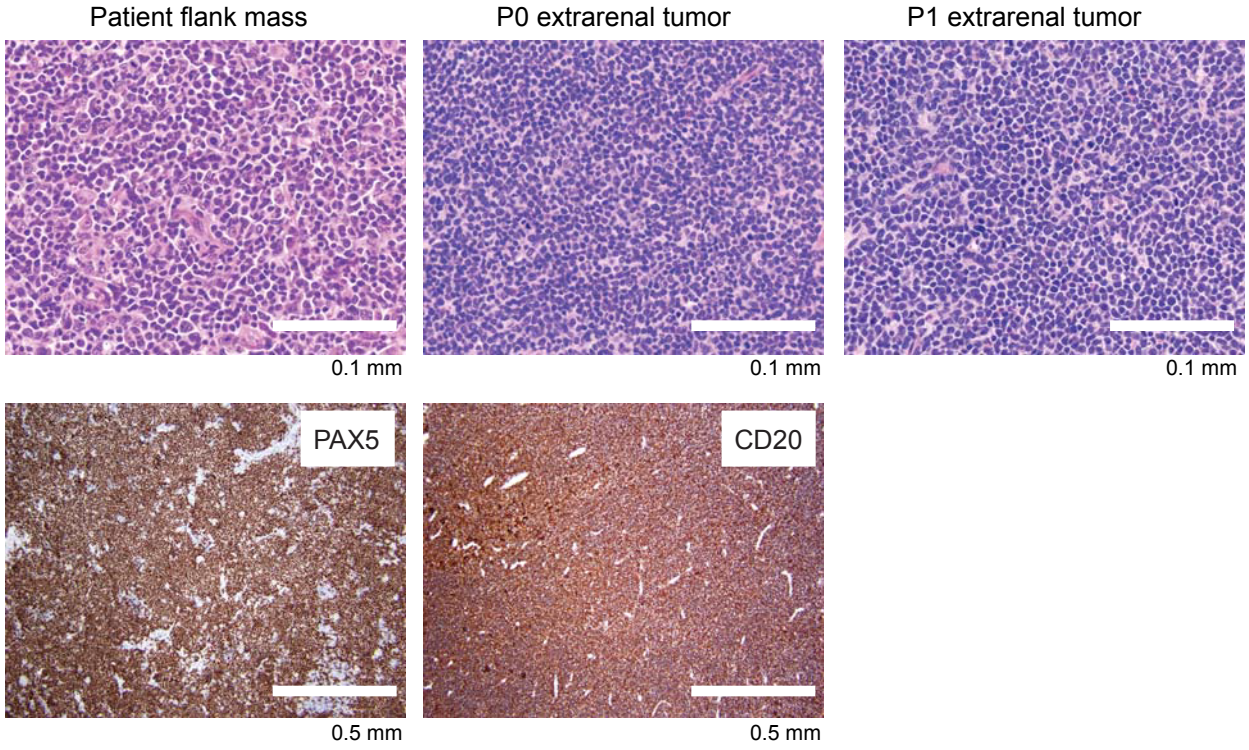
Patient flank mass
P0 extrarenal tumor
P1 extrarenal tumor
0.1 mm
0.1 mm
0.1 mm
PAX5
CD20
0.5 mm
0.5 mm

M

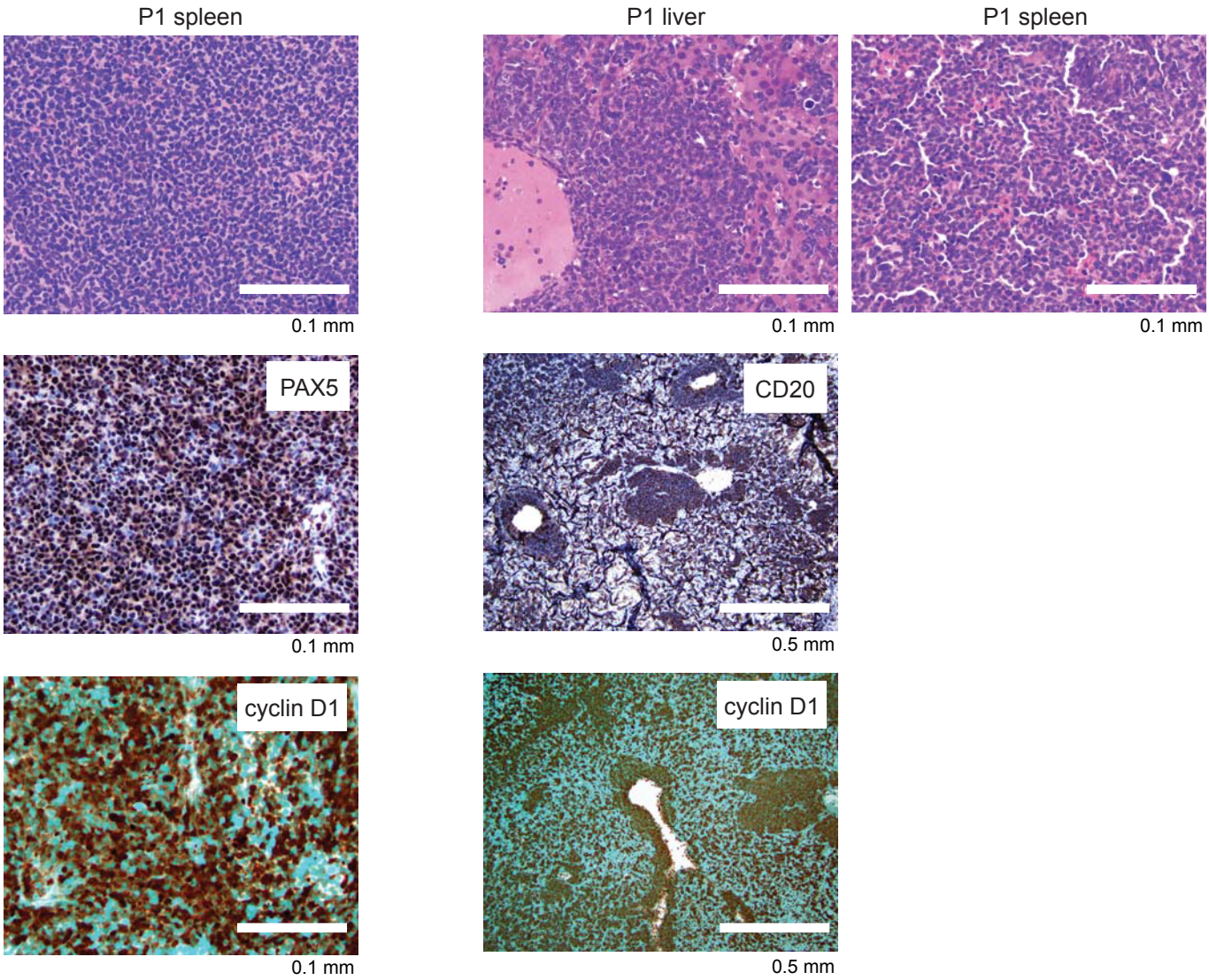
P1 spleen
P1 liver
P1 spleen
0.1 mm
0.1 mm
0.1 mm
PAX5
CD20
0.1 mm
0.5 mm
cyclin D1
cyclin D1
0.1 mm
0.5 mm

Figure S1, refers to Table 1. Phenotypic characterization of xenografts.

(A) Angioimmunoblastic T-cell lymphoma xenograft TL-37237 includes an expanded population of EBV-positive B cells. Top 3 rows: The patient lymph node demonstrated involvement by angioimmunoblastic T-cell lymphoma, characterized by a diffuse infiltrate of small to intermediate-sized atypical CD3-positive T cells with co-expression of PD-1. An infiltrate of morphologically- and immunophenotypically-identical cells was detected in the P0 PDX kidney (site of tumor implant), as well as at distant sites (liver and spleen). Bottom 2 rows: An expanded population of EBV-positive immunoblasts, as highlighted by CD20 and in situ hybridization for EBV-encoded RNA (EBER ISH), was also detected in the patient tumor, a common feature in angioimmunoblastic T-cell lymphoma. This population of EBV-positive B cells formed aggregates in the P0 PDX kidney at the site of tumor implant, but did not spread to the spleen or liver along with the neoplastic T-cell component. All scale bars 0.5 mm.

(B) TL-94393 carries similar histology and identical T cell receptor rearrangement. Hematoxylin and Eosin (H&E) is shown for the patient's original lymph node biopsy and the spleen of a representative mouse with involvement in P1. Nonmalignant $CD7^+$ and $CD8^+$ T cells in the original biopsy are absent in the P1 xenograft. (Below) PCR analysis revealed identical T-cell receptor gene rearrangements in the patient sample and the PDX. Scale bars represent 0.1 mm.

(C) Histology of extranodal NK/T-cell lymphoma (TL-85005). Left column: The patient skin biopsy demonstrated an extensive angiocentric and periadnexal infiltrate of intermediate-sized lymphoid cells with irregular nuclei, vesicular chromatin, variably prominent nucleoli and moderate amounts of cytoplasm. Immunophenotyping revealed a profile indicative of extranodal NK/T-cell lymphoma, including expression of cytoplasmic CD3, CD8 and CD56, and reactivity for EBER ISH. Additional 2 columns: Morphologic and immunophenotypic evaluation of P0 and P1 PDX mice demonstrated identical features, including characteristic lack of surface CD3 expression in the expanded population of CD56-positive cells by flow cytometry. Scale bars represent 0.1 mm.

(D) Breast-implant associated Anaplastic Large Cell Lymphoma (TL-51398). The patient tumor was composed of large-sized cells with pleomorphic nuclei, vesicular chromatin, prominent nucleoli and moderate amounts of eosinophilic cytoplasm which were strongly positive for CD30. Evaluation of the P0 PDX revealed morphologically and immunophenotypically-identical cells at the site of tumor implant as well as in the liver (forming discrete nodules) and in the perisplenic vessels. The P1 PDX tumor maintained the anaplastic morphology. (Below) PCR analysis revealed identical T-cell receptor gene rearrangements in the patient sample and the PDX. Scale bars describe measurements indicated on each panel.

(E) Peripheral T-cell Lymphoma, Not Otherwise Specified (TL-31208). The patient lymph node was effaced by an infiltrate of intermediate to large-sized lymphoid cells with irregular nuclear contours, variably condensed chromatin, distinct nucleoli and small amounts of cytoplasm. Immunophenotyping revealed a CD4-positive T-cell infiltrate with intact expression of CD3 and CD5 and loss of CD7. CD7 and CD8 highlighted background admixed small, reactive T cells. Evaluation of the PDX revealed splenic involvement by a morphologically and immunophenotypically-identical tumor. In addition, scattered CD19-positive B cells of human origin with EBER in situ hybridization reactivity grew in the background of the tumor and the P0 xenograft. PCR analysis revealed identical T-cell receptor gene rearrangements in the patient sample and the PDX. Scale bars represent 0.1 mm.

(F) Blastic Plasmacytoid Dendritic Cell Neoplasm (BPDCN). Flow cytometry of a representative BDPCN represents essentially 100% of cells are $C45^+CD56^+CD123^+$.

(G) Adult T-cell Leukemia Lymphoma (ATLL; TL-69579). Left: Hematoxylin and Eosin (H&E; top) from representative spleen of P0 mouse after tail-vein injection showing characteristic morphology along with $CD3^+CD7^-$ immunophenotype. Right: P0 cells were injected into tail-vein of P1 mice and disease developed in spleen, bone marrow and multiple extramedullary sites. H&E of a representative tumor from the dorsum of a mouse is shown. Scale bars represent 0.1 mm.

(H) Sézary Syndrome (TL-90501). Top panel: The patient skin biopsy showed a predominantly dermal infiltrate of intermediate-sized cells with convoluted nuclear contours, slightly dispersed chromatin, indistinct nucleoli and moderate amounts of cytoplasm. Immunophenotypic analysis revealed an infiltrate composed of CD4-positive T cells with loss of CD7. CD7 and CD8 highlighted background admixed small, reactive T cells. CD3 marked both the

reactive and neoplastic components. Bottom panel: Analysis of the P1 PDX revealed that the tumor cells homed not only to the spleen but also to the mouse skin, filling the dermal space, infiltrating the epidermis and forming multifocal Pautrier microabscesses. The PDX tumor cells showed an identical immunophenotype to the patient specimen. Scale bars describe the measurements indicated.

(I) Diffuse Large B-Cell Lymphoma. BL-86381 demonstrates CNS Tropism (BL-86381). Top Panel: The patient lymph node demonstrated a diffuse infiltrate of large-sized lymphoid cells with irregular nuclear contours, slightly dispersed chromatin, prominent central nucleoli and moderate amounts of pale cytoplasm. Immunophenotyping revealed that the tumor cells were positive for CD19 and CD10, consistent with a diffuse large B-cell lymphoma, germinal center B-cell-like. Additional 3 panels: These morphologic and immunophenotypic features were recapitulated in tumor infiltrates in P0, P1 and P2 PDX mice (immunophenotyping performed by IHC for P0 and P2 PDX mice, and by flow cytometry for P1 PDX mice). The tumor was present at the site of tumor implant in P0 and P1 PDX mice. The P2 PDX mice were generated from tail vein injection of banked cells, and demonstrated extensive CNS spread including involvement of the subpial/subarachnoid space with perivascular extension and superficial infiltration into brain parenchyma (lower right panel). This is a typical distribution pattern for lymphomatous involvement of the brain. Scale bars describe the measurements indicated.

(J) BL-18689 recapitulates bone marrow involvement. Left column: The patient's bone marrow was involved with a DLBCL in 5-10% of cells. After tail-vein injection into P0 mice, disease engrafted in the bone marrow and spleen. H&E and IHC for CD20 in a representative P1 mouse is shown. Scale bars represent indicated measurements.

(K) BL-75549 maintains tissue architecture after serial transplantation under the mouse renal capsule. A tumor seed from spleen involved by a patient's DLBCL was implanted under the renal capsule and expanded in P0 mice. A seed from this extrarenal tumor was then expanded in P1 mice. Representative H&E and IHC are shown. Scale bars represent indicated measurements.

(L) Extranodal marginal zone lymphoma (BL-72516) maintains morphology after serial transplantation under the mouse renal capsule. A patient's flank mass demonstrates effacement by small, $PAX5^{+}$ B-cells that were $CD20^{+}CD5^{-}CD23^{-}$ (not shown). Morphology is maintained after serial transplantation of tumor seeds under the renal capsule of P0 and P1 mice. Scale bars represent indicated measurements.

(M) Mantle cell lymphomas involving the blood readily engraft and metastasize to extramedullary sites**.** Left panel: BL-96069 was generated by tail-vein injection of peripheral blood from a patient with peripheral blood involvement by MCL and grew in bone marrow, peripheral blood and spleen. Right panel: Similarly, BL-98848 was generated by tail-vein injection of blood from a 2^{nd} patient and involved bone marrow, blood, spleen and metastasized to liver. H&E and IHC are shown from representative mice. Scale bars represent indicated measurements. A third MCL model (BL-39435; see Movie S1, provided as a separate file) involved blood, bone marrow, lymph nodes, spleen, and gastrointestinal tract of P1 mice.

Movie S1, refers to Table 1. ^{18}F-FLT PET of a representative NSG mouse xenografted with BL-39435 obtained 23 days after transplantation. Disease is visible based on tracer uptake in multiple nodal regions, gastrointestinal tract, proximal femurs, sternum and spleen. Provided as a separate movie (.avi) file.

Table S1, refers to Figure 1. Gene list for targeted exon sequencing.

ABCA7	*CARD11*	*DDX3X*	*ID3*	*MKI67*	*PIGA*	*SETBP1*	*TCF3*
ABL1	*CBL*	*DIS3*	*IDH1*	*MLL3*	*PIK3AP1*	*SETD2*	*TCF4*
ALMS1	*CCND1*	*DNMT3A*	*IDH2*	*MLL2*	*PIK3CA*	*SF1*	*TET2*
ALPK2	*CCND2*	*EBF1*	*IKZF1*	*MLL3*	*PIK3CD*	*SF3A1*	*TLR2*
APC	*CCND3*	*EED*	*IKZF2*	*MUM1*	*PIK3R1*	*SF3B1*	*TNFAIP3*
ARID1A	*CD200*	*EP300*	*IKZF3*	*MYC*	*PIM1*	*SGK1*	*TNFRSF14*
ARID1B	*CD36*	*EPHA6*	*IL7R*	*MYCN*	*PLCG2*	*SH2B3*	*TNFSF9*
ARID2	*CD58*	*EPHA7*	*IRAK1*	*MYD88*	*POT1*	*SMARCA2*	*TP53*
ARID3A	*CD79A*	*ETS1*	*IRF4*	*NF1*	*PRDM1*	*SMARCA4*	*TP63*
ASXL1	*CD79B*	*ETV6*	*IRF8*	*NFKB2*	*PRDM16*	*SMARCB1*	*TP73*
ATM	*CDK4*	*EZH2*	*JAK1*	*NFKBIA*	*PRKDC*	*SMC1A*	*TRAF2*
ATRX	*CDK6*	*FAS*	*JAK2*	*NLRP5*	*PRPF8*	*SMC3*	*TRAF3*
B2M	*CDKN2A*	*FBXO11*	*JAK3*	*NOTCH1*	*PTEN*	*SOCS1*	*TRAF6*
BACH2	*CDKN2B*	*FBXW7*	*KDM4C*	*NOTCH2*	*PTPN11*	*SRSF2*	*TYK2*
BCL10	*CEBPA*	*FLT3*	*KDM6A*	*NOTCH3*	*RAD21*	*SRSF6*	*U2AF1*
BCL11A	*CELSR2*	*FOXO1*	*KIT*	*NPM1*	*RAPGEF1*	*SRSF8*	*U2AF2*
BCL11B	*CHD2*	*GATA1*	*KLHL6*	*NR3C1*	*RB1*	*STAG2*	*UBR5*
BCL2	*CIITA*	*GATA2*	*KRAS*	*NRAS*	*REL*	*STAT1*	*ULK4*
BCL6	*CNOT3*	*GATA3*	*LEF1*	*NT5C2*	*RELN*	*STAT3*	*VPS13A*
BCL7A	*CREBBP*	*GNA11*	*LMO2*	*P2RY8*	*RFTN1*	*STAT5A*	*WT1*
BCR	*CRLF2*	*GNA13*	*LUC7L2*	*PAX5*	*RHOA*	*STAT5B*	*XPO1*
BLNK	*CSF1R*	*GNAQ*	*MALT1*	*PCLO*	*RNF213*	*STAT6*	*ZFHX3*
BRAF	*CSF3R*	*GNAS*	*MDM2*	*PDGFC*	*RPL10*	*SUZ12*	*ZRSR2*
BTG1	*CTCF*	*GNB1*	*MDM4*	*PDGFRA*	*RPL5*	*SYK*	
BTG2	*CTSS*	*GNB2*	*MEF2B*	*PDGFRB*	*RUNX1*	*TAL1*	
BTK	*CXCR4*	*HCK*	*MEF2C*	*PHF6*	*SENP6*	*TBL1XR1*	

205 genes that were sequenced using an established next-generation sequencing platform (Odejide et al Blood 2014) in PDXs

Table S2, refers to Figure 1. Mutation calls from 205 genes sequenced in 107 PDXs. Provided as separate excel file.

A

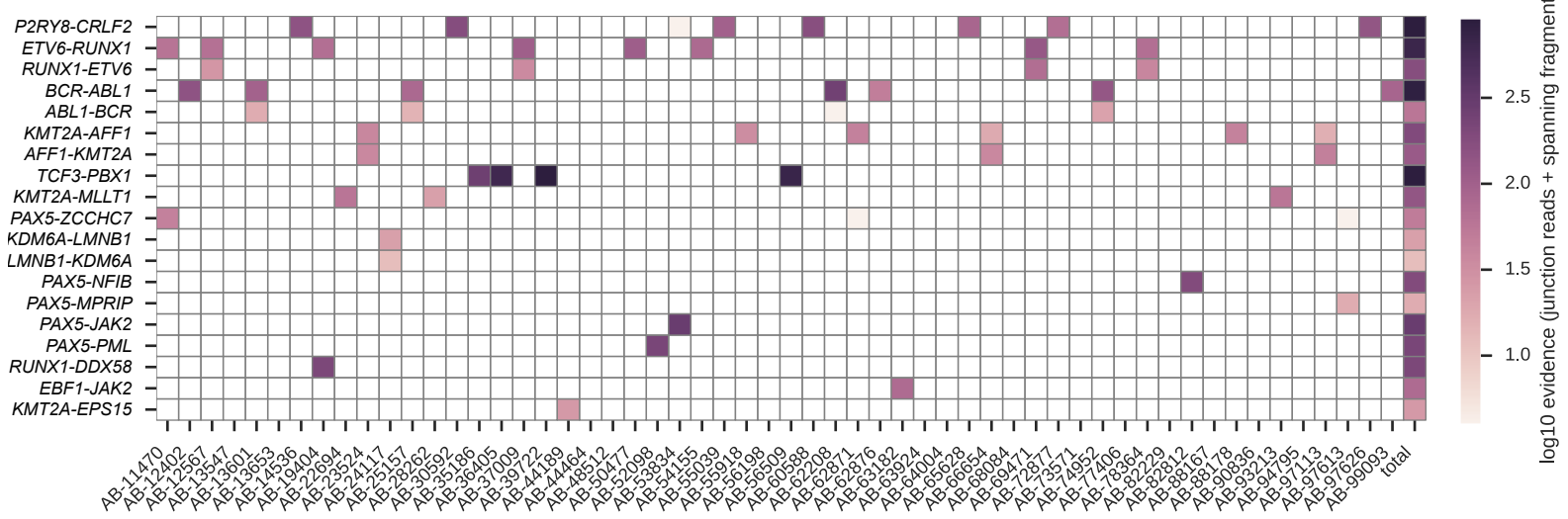
P2RY8-CRLF2
ETV6-RUNX1
RUNX1-ETV6
BCR-ABL1
ABL1-BCR
KMT2A-AFF1
AFF1-KMT2A
TCF3-PBX1
KMT2A-MLLT1
PAX5-ZCCHC7
KDM6A-LMNB1
LMNB1-KDM6A
PAX5-NFIB
PAX5-MPRIP
PAX5-JAK2
PAX5-PML
RUNX1-DDX58
EBF1-JAK2
KMT2A-EPS15
AB-11470
AB-12402
AB-12567
AB-13547
AB-13601
AB-13653
AB-14536
AB-19404
AB-22694
AB-23524
AB-24117
AB-25157
AB-28262
AB-30592
AB-35186
AB-36405
AB-37009
AB-39722
AB-44189
AB-44464
AB-48512
AB-50477
AB-52098
AB-53834
AB-54155
AB-55039
AB-55918
AB-56198
AB-56509
AB-60588
AB-62208
AB-62871
AB-62876
AB-63182
AB-63924
AB-64004
AB-65628
AB-66654
AB-68084
AB-69471
AB-72877
AB-73571
AB-74952
AB-77406
AB-78364
AB-82229
AB-82812
AB-88167
AB-88178
AB-90836
AB-93213
AB-94795
AB-97113
AB-97613
AB-97626
AB-99093
total
2.5
2.0
1.5
1.0
log10 evidence (junction reads + spanning fragments)

B

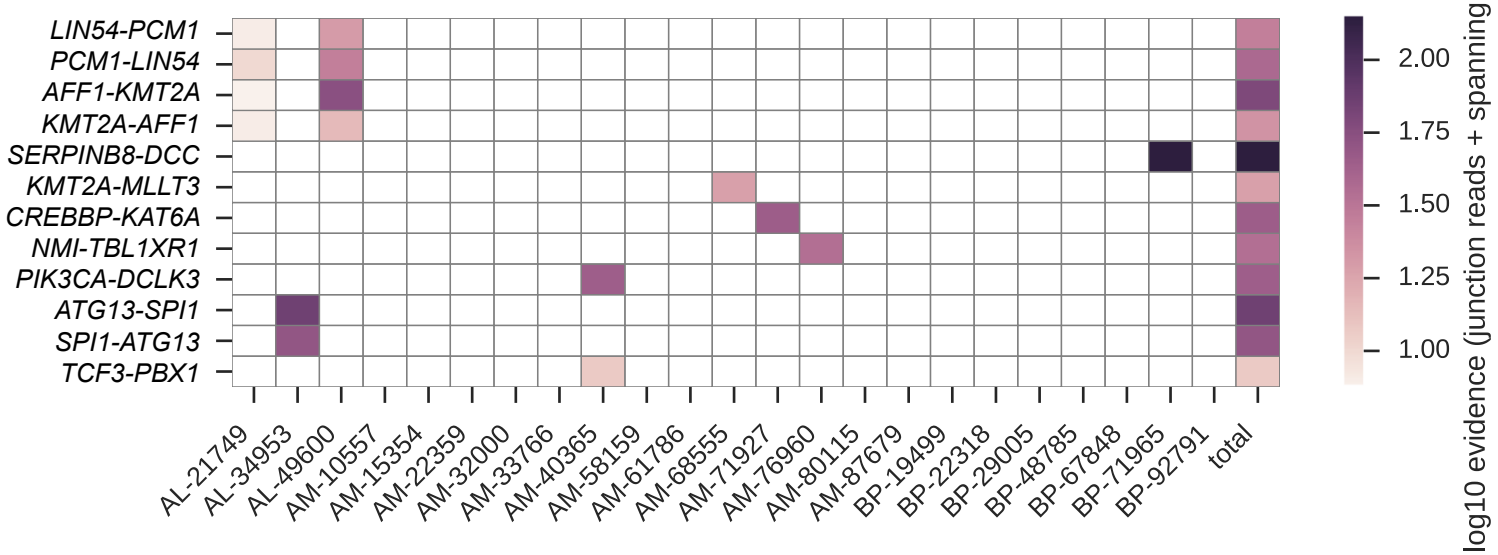
LIN54-PCM1
PCM1-LIN54
AFF1-KMT2A
KMT2A-AFF1
SERPINB8-DCC
KMT2A-MLLT3
CREBBP-KAT6A
NMI-TBL1XR1
PIK3CA-DCLK3
ATG13-SPI1
SPI1-ATG13
TCF3-PBX1
AL-21749
AL-34953
AL-49600
AM-10557
AM-15354
AM-22359
AM-32000
AM-33766
AM-40365
AM-58159
AM-61786
AM-68555
AM-71927
AM-76960
AM-80115
AM-87679
BP-19499
BP-22318
BP-29005
BP-48785
BP-67848
BP-71965
BP-92791
total
2.00
1.75
1.50
1.25
1.00
log10 evidence (junction reads + spanning fragments)


C
a
b
cohort
WHO−classification
Phase of Treatment
Gender
Age
Cytogenetic Risk Category
FAB Classification
c
Allogeneic HSCT
Chemotherapy
Hydroxyurea
Hypomethylating therapy
Molecular therapy
None
10 30 50 70
d
Normal
MLL−Rearranged
t(9;22) BCR−ABL1
t(15;17) PML−RARA
t(8;21) RUNX1−RUNX1T1
inv(16) CBFB−MYH11
Complex
Hyperdiploid
add(5q), del(5q), −5
add(7q), del(7q), −7
+8
abn(9p)
abn(11q), +11
add(13q), del(13q), −3
+21/iAMP21
Not Available
0 20 40 60
e
JAK2
KRAS
CBL
NRAS
KIT
PTPN11
FLT3
NOTCH1
DNMT3A
TET2
IDH1
IDH2
CEBPA
RUNX1
ASXL1
U2AF1
ZRSR2
TP53
WT1
NPM1
ABL1
RB1
MLL2
MYD88
GNB1
0 2 4 6 8
Legend
RNA Expression z−score
3
2
1
0
−1
Sample Cohort
CCLE
PDX
TCGA
Disease WHO−classification
AML NOS
AML Therapy−Related
AML with inv(16) CBFB−MYH11
AML with MDS−related changes
AML with MLL rearrangement
AML with recurrent gene mutations
AML with t(15;17) PML−RARA
AML with t(8;21) RUNX1−RUNX1T1
AML with t(9;11) MLLT3−MLL
AML with variant MLL translocation
B/myeloid acute leukemia
BPDCN
Insufficient information to classify
LAL with t(v;11q23) MLL rearranged
MDS refractory cytopenias with multilineage dysplasia
Disease Phase of Treatment
Data not available
Primary refractory
Refractory
Relapse
Untreated
Patient Gender
F
M
Patient Age (Years)
0−9
10−17
18−39
40−64
65−79
80+
AML Cytogenetic Risk Category
Adverse
Favorable
Intermediate
Not available
[Not Available]
Poor
Unable to assess
AML FAB Classification
M0
M1
M2
M3
M4
M5
M5a
M7
Not Classified
PDX Mutations
Dominant negative mutation
Frame Shift Deletion
Frame Shift Insertion
ITD
Missense
Nonsense
Not specified
Structural variant
Type A

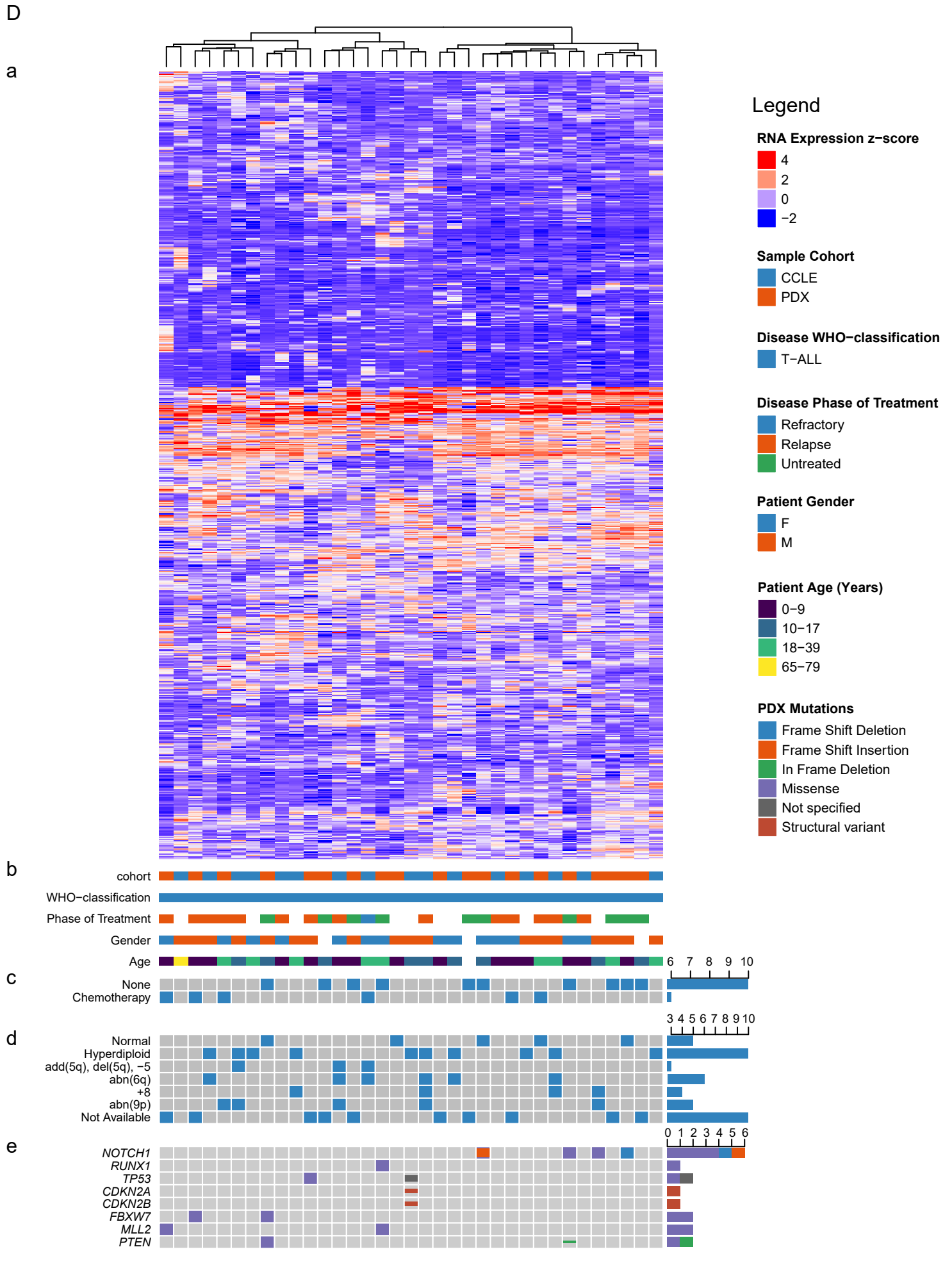
D
a
b
c
d
e
Legend
RNA Expression z−score
4
2
0
−2
Sample Cohort
CCLE
PDX
Disease WHO−classification
T−ALL
Disease Phase of Treatment
Refractory
Relapse
Untreated
Patient Gender
F
M
Patient Age (Years)
0−9
10−17
18−39
65−79
PDX Mutations
Frame Shift Deletion
Frame Shift Insertion
In Frame Deletion
Missense
Not specified
Structural variant
cohort
WHO−classification
Phase of Treatment
Gender
Age
6 7 8 9 10
None
Chemotherapy
3 4 5 6 7 8 9 10
Normal
Hyperdiploid
add(5q), del(5q), −5
abn(6q)
+8
abn(9p)
Not Available
0 1 2 3 4 5 6
NOTCH1
RUNX1
TP53
CDKN2A
CDKN2B
FBXW7
MLL2
PTEN

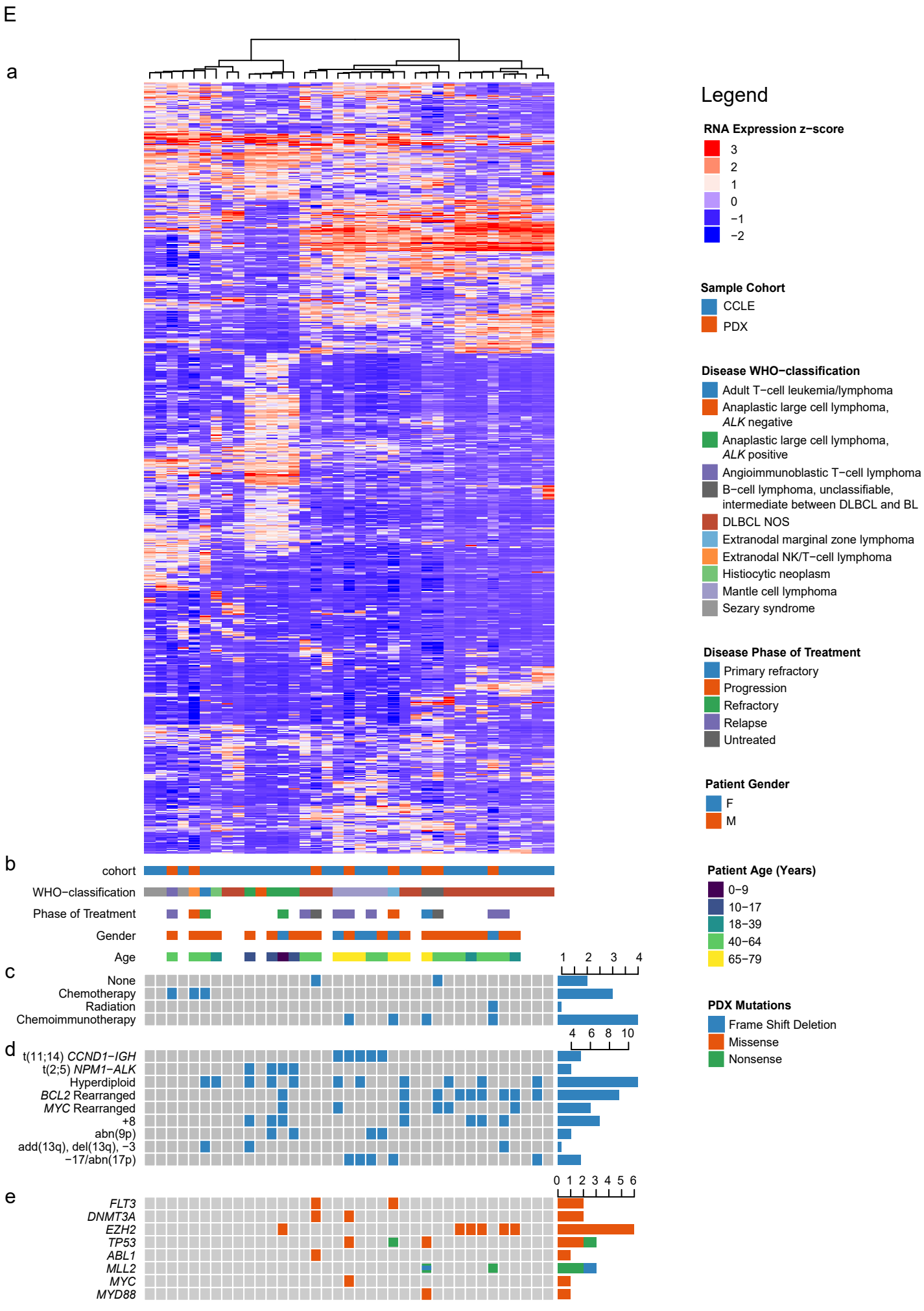
E
a
b
cohort
WHO−classification
Phase of Treatment
Gender
Age
c
None
Chemotherapy
Radiation
Chemoimmunotherapy
1 2 3 4
d
t(11;14) CCND1−IGH
t(2;5) NPM1−ALK
Hyperdiploid
BCL2 Rearranged
MYC Rearranged
+8
abn(9p)
add(13q), del(13q), −3
−17/abn(17p)
4 6 8 10
e
FLT3
DNMT3A
EZH2
TP53
ABL1
MLL2
MYC
MYD88
0 1 2 3 4 5 6
Legend
RNA Expression z−score
3
2
1
0
−1
−2
Sample Cohort
CCLE
PDX
Disease WHO−classification
Adult T−cell leukemia/lymphoma
Anaplastic large cell lymphoma, ALK negative
Anaplastic large cell lymphoma, ALK positive
Angioimmunoblastic T−cell lymphoma
B−cell lymphoma, unclassifiable, intermediate between DLBCL and BL
DLBCL NOS
Extranodal marginal zone lymphoma
Extranodal NK/T−cell lymphoma
Histiocytic neoplasm
Mantle cell lymphoma
Sezary syndrome
Disease Phase of Treatment
Primary refractory
Progression
Refractory
Relapse
Untreated
Patient Gender
F
M
Patient Age (Years)
0−9
10−17
18−39
40−64
65−79
PDX Mutations
Frame Shift Deletion
Missense
Nonsense

Figure S2, refers to Figure 1.

(A) Gene fusions identified in B-ALL PDX models based on transcriptome sequencing. Candidate fusions were called from RNA-Seq data using the STAR-Fusion 0.4.0 algorithm (https://star-fusion.github.io) and quantitatively evaluated by summing spanning fragments and junction reads. Those with sums of ≥10 over all samples were retained and manually filtered to remove likely homology-induced artifacts. Fusions detected in B-ALL PDX models are depicted here in heatmap form, with color coding for strength of evidence supporting fusion calls. Both canonical and reciprocal fusions (e.g., *BCR-ABL1* and *ABL1-BCR*) are shown, when detected. PDX samples are ordered alphanumerically to facilitate sample identification.

(B) Gene fusions identified in AML PDX models based on transcriptome sequencing. Candidate fusions were called from RNA-Seq data and filtered as described. Fusions detected in AML PDX models are depicted here in heatmap form, with color coding for strength of evidence supporting fusion calls. Both canonical and reciprocal fusions (e.g., *KMT2A-AFF1* and *AFF1-KMT2A*) are shown, when detected. PDX samples are ordered alphanumerically.

(C) Integrative analysis of AML PDX models, primary samples, and cell lines. (a) Unsupervised hierarchical clustering of RNA expression profiles among 20 AML PDX models (PDX cohort), 104 external primary AML samples (TCGA cohort), and 20 AML cell lines (CCLE cohort), using the same methods as for figure 1. (b) Key clinical characteristics of patients from whose tumors PDX models (PDX cohort) or cell lines (CCLE cohort) were derived, or whose tumors were sequenced directly (TCGA cohort), including specific diagnosis (by WHO 2008 classification), phase of treatment (as previously defined in Figure 1 legend), patient gender, patient age when the referenced tumor specimen was obtained, FAB classification (for historical reference), and cytogenetic risk category (using criteria of (Grimwade et al., 2010)). (c) Binary matrix of prior therapies to which patient was exposed prior to sampling of the referenced tumor, if known. (d) Selected cytogenetic features of patient tumors from which PDX models (PDX cohort) or cell lines (CCLE cohort) were derived, or of the tumors themselves (TCGA cohort). Shown are cytogenetic features or groups of related features reported in at least three samples within this data set. (e) OncoPrint of selected mutations detected in PDX models by targeted exon sequencing, reported in cell lines by ATCC or DSMZ or reported in primary samples within the clinical annotation available from TCGA. Overall, AML clustering tended to reflect cytogenetic changes, with t(15;17) M3 AMLs forming a distinct clade, as with pediatric t(8;21) M1/M2 AMLs and AMLs with MDS-related cytogenetic changes. Of note, our repository includes nine blastic plasmacytoid dendritic cell neoplasms (BPDCN), of which seven underwent whole transcriptome sequencing; these, too, formed a tight cluster.

(D) Integrative analysis T-ALL PDX models and cell lines. (a) Unsupervised hierarchical clustering of RNA expression profiles among 19 T-ALL PDX models (PDX cohort) and 16 T-ALL cell lines (CCLE cohort), using the same methods as for figure 1. (b) Key clinical characteristics of patients from whose tumors PDX models (PDX cohort) or cell lines (CCLE cohort) were derived, including specific diagnosis (by WHO 2008 classification), phase of treatment (as previously defined in Figure 1 legend), patient gender, and patient age when the referenced tumor specimen was obtained. (c) Binary matrix of prior therapies to which patient was exposed prior to sampling of the referenced tumor, if known. (d) Selected cytogenetic features of patient tumors from which PDX models (PDX cohort) or cell lines (CCLE cohort) were derived. Shown are cytogenetic features or groups of related features reported in at least three samples within this data set. (e) OncoPrint of selected mutations detected in PDX models by targeted exon sequencing or reported in cell lines by ATCC or DSMZ. Overall, T-ALLs comprised two primary clusters, one enriched in samples with isolated *NOTCH1* mutations, and the other with mutations in various other genes, including *FBXW7*.

(E) Integrative analysis of non-Hodgkin lymphoma PDX models and cell lines. (a) Unsupervised hierarchical clustering of RNA expression profiles among 8 non-Hodgkin lymphoma PDX models (PDX cohort) and 29 non-Hodgkin lymphoma cell lines (CCLE cohort), using the same methods as for figure 1. (b) Key clinical characteristics of patients from whose tumors PDX models (PDX cohort) or cell lines (CCLE cohort) were derived, including specific diagnosis (by WHO 2008 classification), phase of treatment (as previously defined in Figure 1 legend), patient gender, and patient age when the referenced tumor specimen was obtained. (c) Binary matrix of prior therapies to which patient was exposed prior to sampling of the referenced tumor, if known. (d) Selected cytogenetic features of patient tumors from which PDX models (PDX cohort) or cell lines (CCLE cohort) were derived. Shown are cytogenetic features or groups of related features reported in at least three samples within this data set. (e) OncoPrint of selected mutations detected in PDX models by targeted exon sequencing or reported in cell lines by ATCC or DSMZ.

Table S3, refers to Figure 1. PDXs arranged in the same order as on the Y axis of the transcriptional heatmap and genes arranged in the same order as the X axis of the transcriptional heatmap for all PDXs in Figure 1. Provided as separate excel file.

Table S4, refers to Figure 2. PDXs arranged in the same order as on the Y axis of the transcriptional heatmap and gene arranged in the same order as the X axis of the transcriptional heatmap for B-ALL samples (PDXs, cell lines and primary samples). Provided as separate excel file.

A

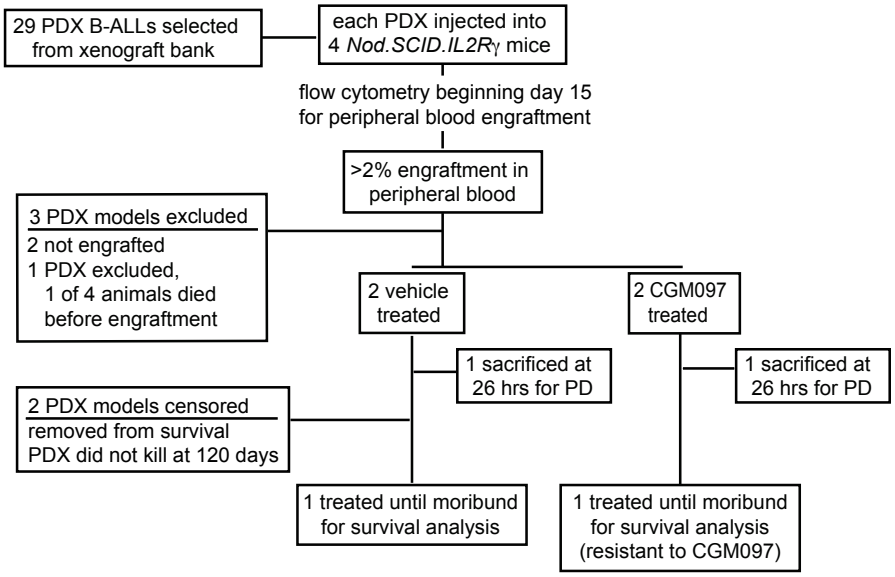

B

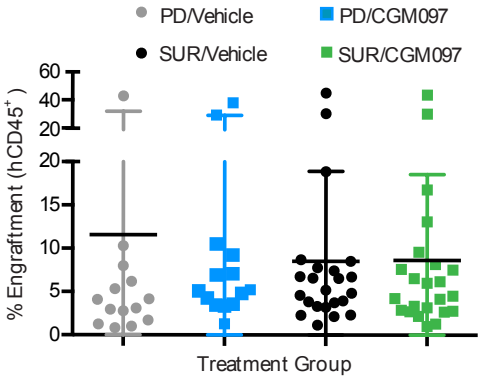

C

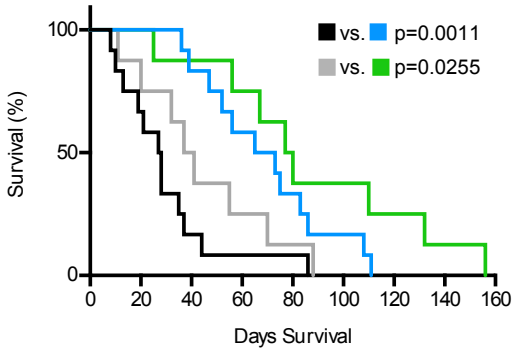

	Patient Sex	Treatment	n	Median Surv .
	female	vehicle	12	27.5
	female	CGM097	12	69
	male	vehicle	8	39
	male	CGM097	8	78.5

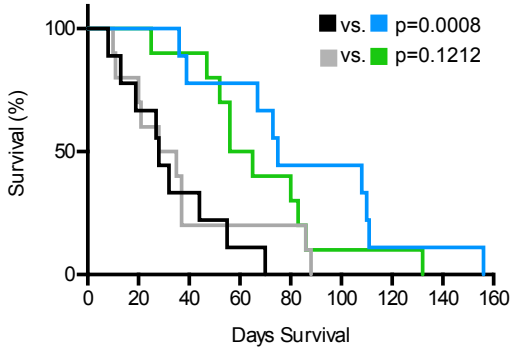

	Patient Age	Treatment	n	Median Surv .
	pediatric (<18)	vehicle	9	28
	pediatric (<18)	CGM097	9	75
	adult (>=18)	vehicle	10	31.5
	adult (>=18)	CGM097	10	60.5

Figure S3, refers to Figure 3.

(A) Study design of CGM097 survival study. 29 B-ALL PDXs were engrafted into 4 Nod. SCID.*IL2R*γ mice. After engraftment, animals were randomized to vehicle and treatment cohorts. 5 PDX models were excluded from the final data set for failure to meet previously established study criteria. Animals were dosed daily by oral gavage with 100mg/kg CGM097 or methycellulose vehicle.

(B) Xenograft engraftment characteristics for CGM097 survival study. Peripheral blood engraftment after red blood cell lysis of animals for each treatment cohort as determined by flow cytometry for human CD19 and human CD45.

(C) Kaplan-Meier survival analysis of *TP53* wild-type PDX models derived from female patients or male patients (left) and pediatric patients versus adult patients (right). Comparison was performed using the log-rank test.

Error bars represent the standard error of the mean (S.E.M.).

Table S5, refers to Figure 4. List of genes in the Nanostring ETP53 Panel.

ABCB1	*CHEK2*	*IGFBP4*	*SESN1*
ACTA2	*COL18A1*	*ITSN1*	*SESN2*
AEN	*CPB2*	*KAT2B*	*SESN3*
AKT1S1	*CRY1*	*LRDD*	*SFN*
APAF1	*CSNK1A1*	*MAPK8*	*SHISA5*
ATF3	*CSNK1D*	*MCL1*	*SIAH1*
ATM	*DDB2*	*MDM2*	*SIAH2*
ATR	*E2F1*	*MDM4*	*SIAH3*
BAI1	*E2F3*	*MRAS*	*SIRT1*
BAX	*FAS*	*NFKBIB*	*ST13*
BBC3	*FDXR*	*NQO1*	*STEAP3*
BCL2	*FHL2*	*PCNA*	*THBS1*
BCL6	*GADD45A*	*PERP*	*TIMP3*
BID	*GAK*	*PIGS*	*TNFRSF10B*
BRCA1	*GAL3ST3*	*PLK3*	*TP53*
BTG2	*GDF15*	*PMAIP1*	*TP63*
CASP2	*GTSE1*	*PPM1D*	*TP73*
CASP3	*HDAC1*	*PRKAB1*	*TSC2*
CASP8	*HIC1*	*PTEN*	*UQCRFS1*
CASP9	*HIF1A*	*PTK2*	*VCAN*
CCND1	*HRAS*	*RB1*	*XPC*
CCNE1	*HSF1*	*RCHY1*	*ZMAT3*
CCNG1	*HSP90AA1*	*RDBP*	***CLTC***
CDK1	*HSPA1A*	*RFWD2*	***GAPDH***
CDK2	*HSPA1B*	*RPRM*	***GUSB***
CDK4	*HSPA4L*	*RPS27L*	***HPRT1***
CDK6	*HSPA8*	*RRM2B*	***PGK1***
CDKN1A	*IER3*	*SERPINB2*	***TUBB***
CDKN2A	*IGFBP1*	*SERPINB5*	*mGapdh*
CHEK1	*IGFBP3*	*SERPINE1*	*mPgk1*

Housekeeping genes for normalization are indicated in **bold**. Murine *Gapdh* and *Pgk1* are included to measure contamination by murine cells.

Table S6, refers to Figure 4. Differentially expressed genes in *TP53* wild-type PD samples

Gene	Mean Vehicle	Mean CGM097	Fold Change	p value	FDR
BBC3	134	694	5.18	1.31E-11	4.46E-10
TNFRSF10B	234	790	3.37	3.08E-06	5.24E-05
ZMAT3	734	2617	3.56	8.77E-06	9.94E-05
FAS	69	225	3.27	6.57E-05	4.93E-04
CDKN1A	2838	7823	2.76	7.25E-05	4.93E-04
MDM2	9527	20079	2.11	3.56E-04	2.02E-03
FDXR	58	138	2.37	5.18E-04	2.52E-03
LRDD	274	367	1.34	1.09E-02	4.63E-02
SESN2	59	118	2.01	1.31E-02	4.95E-02
AEN	101	200	1.98	1.95E-02	6.63E-02
DDB2	331	584	1.77	2.31E-02	7.14E-02
SESN1	145	291	2.01	2.57E-02	7.17E-02
BAX	1399	2643	1.89	2.74E-02	7.17E-02
GAL3ST3	4	3	0.61	3.21E-02	7.34E-02
CDK1	5127	2984	0.58	3.24E-02	7.34E-02
XPC	334	586	1.76	4.70E-02	9.99E-02

PDX models were treated for 26 hrs with CGM097 versus vehicle. Differentially expressed genes were identified using DESeq, genes that had an unadjusted p value <0.05 are shown. Genes with FDR <0.05 are in blue.

Table S7, refers to Figure 4. Differentially expressed genes in CGM097-treated samples at early treatment and after disease progression.

Gene	Mean PD	Mean SUR	Fold Change	p value	FDR
TNFRSF10B	940	376	0.4	0.00247	0.00846
BBC3	805	311	0.39	0.00282	0.00846
FAS	269	104	0.39	0.00749	0.01498
FDXR	164	76	0.46	0.02929	0.04265
MDM2	22999	13251	0.58	0.03638	0.04265
CDKN1A	9060	4527	0.5	0.04265	0.04265

Differentially expressed genes in CGM097-treated *TP53* wild-type PDX models at 26 hrs (PD) versus moribund (SUR) timepoints. Differentially expressed genes were identified using DESeq, genes that had a p value <0.05 are shown and all had FDR < 0.05.

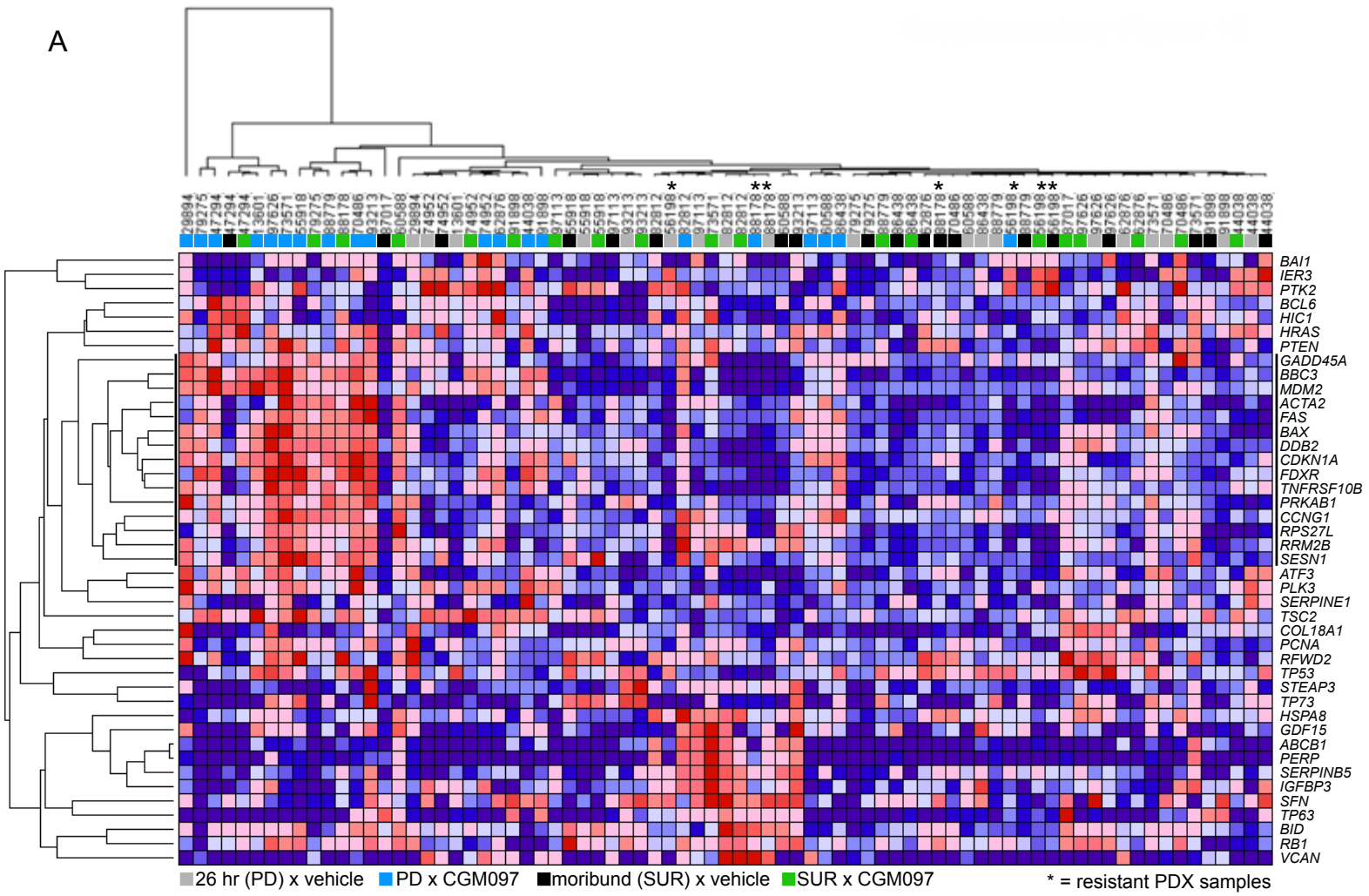
A
BAI1
IER3
PTK2
BCL6
HIC1
HRAS
PTEN
GADD45A
BBC3
MDM2
ACTA2
FAS
BAX
DDB2
CDKN1A
FDXR
TNFRSF10B
PRKAB1
CCNG1
RPS27L
RRM2B
SESN1
ATF3
PLK3
SERPINE1
TSC2
COL18A1
PCNA
RFWD2
TP53
STEAP3
TP73
HSPA8
GDF15
ABCB1
PERP
SERPINB5
IGFBP3
SFN
TP63
BID
RB1
VCAN
26 hr (PD) x vehicle
PD x CGM097
moribund (SUR) x vehicle
SUR x CGM097
* = resistant PDX samples

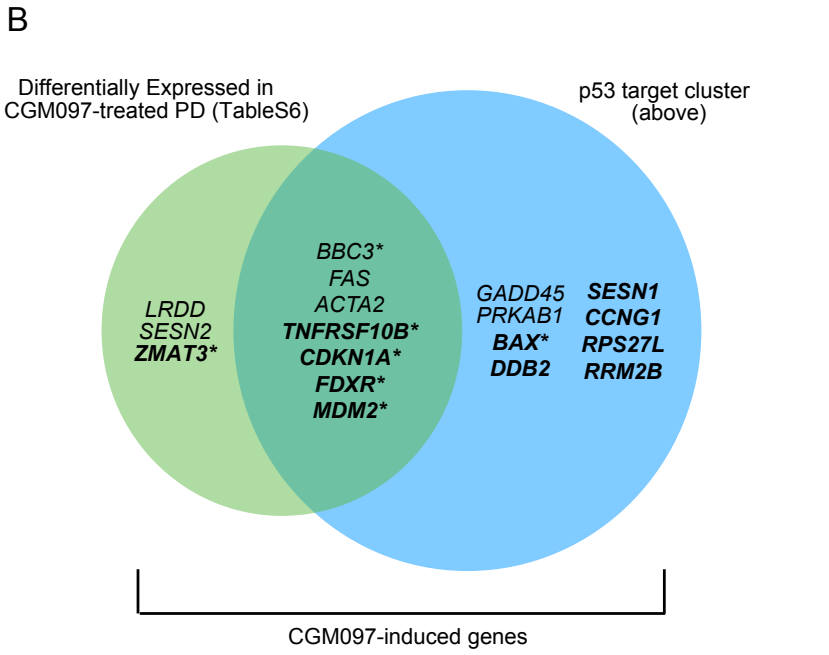
B
Differentially Expressed in CGM097-treated PD (TableS6)
p53 target cluster (above)
LRDD
SESN2
ZMAT3*
BBC3*
FAS
ACTA2
TNFRSF10B*
CDKN1A*
FDXR*
MDM2*
GADD45
PRKAB1
BAX*
DDB2
SESN1
CCNG1
RPS27L
RRM2B
CGM097-induced genes
Bold = 13 Gene Signature genes (Jeay et al. eLife 2015)
* = upregulated in RG7112-treated patients (Andreef et al Clin. Canc. Res 2015)

Figure S4, refers to Figure 4.

(A) Heatmap of genes on the NanoString set and samples obtained from mice treated with vehicle or CGM097 at both the PD (26 hours) and SUR (moribund timepoints).

(B) Venn diagram overlaying genes differentially expressed in CGM097-treated PDXs at the PD timepoint (green), as determined by DESeq (Table S6) and genes within the p53 target cluster (identified as a cluster in red in the upper left of the heatmap above). Genes in bold were among the 13 identified within the response signature of cell lines to CGM097 by Jeay et al. eLife 2015. Those with * were among the genes identified as modulated by RG7112 in patient samples by Andreeff et al. Clin Cancer Res 2015.

Supplemental Experimental Procedures

CGM097 Study

Viably frozen B-ALL xenograft cells were thawed and changed into 1X PBS before tail-vein injection at 0.5-2.0x10^6 per mouse. Engraftment was monitored every 7 days, starting 3 weeks post-injection, by flow cytometry of 50 µl of peripheral blood. Blood was processed with Red Blood Cell Lysis Buffer (Qiagen) before staining with antibodies against human CD45 (APC-conjugated, eBioscience 17-0459-42) and human CD19 (PE-conjugated eBioscience 12-0193-82) in 1XPBS with 2mM EDTA to assess engraftment. Flow cytometry data was analyzed with FlowJo. When engraftment was determined to be ≥ 2% of the live cell population, the remaining two animals with the same PDX were bled for analysis before starting treatment. Animals were dosed daily with 100 mg/kg CGM097 or methylcellulose vehicle by oral gavage.

Pharmacodynamic assessment

26 hours after the start of treatment (2 hours after receiving the second drug dose), animals were euthanized according to standard IACUC approved protocols. Spleens were removed and a section was fixed in 10% paraformaldehyde for immunohistochemistry along with one femur. The remaining splenocytes were mechanically disrupted, red blood cell lysed and depleted of mouse cells by magnetic bead sorting. Cells were divided into 1-5x10^6/cell aliquots and snap frozen for further analysis.

Statistical Methods

Data were collected using the nCounter Digital Analyzer. Raw NanoString counts were normalized in NSolver using positive control probe sets followed by a biological normalization with six housekeeping genes and subtraction of negative controls for background noise see Table S5 for gene list. Normalization diagnostics were also examined using the NanoStringNorm package in R. Unsupervised clustering analysis was performed using Pearson correlation with average link clustering. Differential expression between experimental criteria was determined using raw counts and normalization procedures within the DEseq package in R based on a negative binomial distribution. The false discovery rate (FDR – Benjamini and Hochberg) method was used to adjust for multiple comparisons after filtering for those in which at least a 1.2 fold change was observed. Both unsupervised and supervised clustering were performed using GenePattern (Broad Institute).

RNASeq

Analysis of RNASeq data was implemented as a Snakemake (Koster and Rahmann, 2012) workflow. The complete workflow documenting all utilized parameters and tools so as to permit reproducibility is available at https://bitbucket.org/cfce/weinstock-leukemia. Paired end RNASeq samples were mapped to the human genome reference assembly (hg19) with STAR 2.4.2a (Dobin et al., 2013). Transcript expressions were estimated with Cufflinks 2.2.1 without transcript assembly (Trapnell et al., 2010). Gene expressions were calculated as sums of transcript FPKM values. Genes with transcripts smaller than 300bp were ignored. In order to compare the obtained FPKM values with external datasets, namely RNASeq RPKMs from the TCGA AML cohort, RMA-normalized log2 scaled microarray intensities from CCLE cohort and RNASeq RPKMs from NCBI Sequence Read Archive (SRA) study SRP058414 (primary human pre-B ALL whole transcriptome sequencing, http://www.ncbi.nlm.nih.gov/Traces/study/?acc=SRP058414). All expression values were log2 transformed.

Pre-normalized gene expressions follow similar bimodal distributions in all data sets. A quantile normalization (Limma 3.26.1 (Ritchie et al., 2015)) was therefore performed to adjust for library depth and technology specific differences, as shown below. Distribution of gene expressions in log2 scale derived from multiple data sets (CCLE

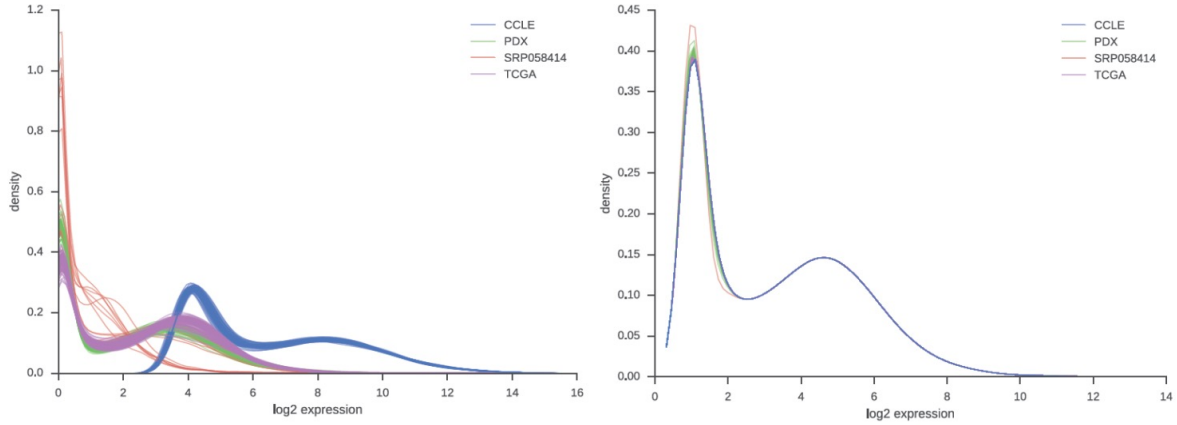

cell lines, PDX models, SRP058414 primary pre-B ALL samples, and TCGA primary AML samples). Data are shown before (left panel) and after (right panel) quantile normalization. The primary sources of variation after quantile normalization were the different batches (see below).

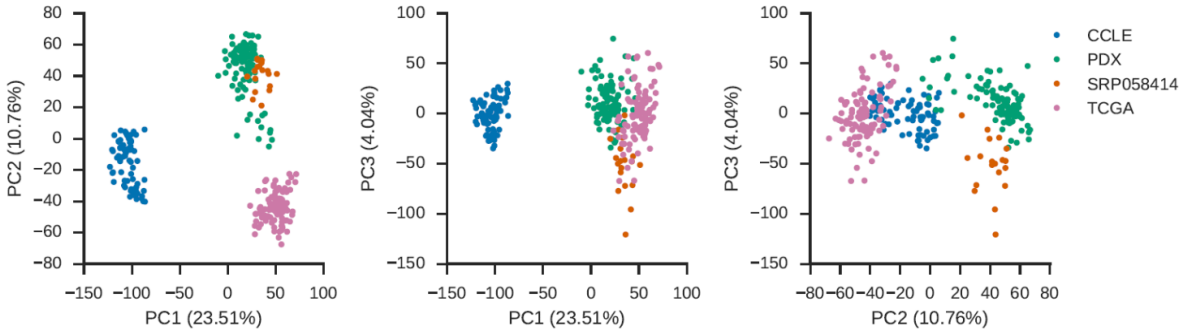

For the histology specific analysis, we successfully removed batch effects within each tumor type using the ComBat approach from SVA 3.18.0 (http://doi.org/10.1038/nbt.1621) without specifying additional covariates. Shown above is the principle components analysis of quantile-normalized gene expression from multiple data sets (CCLE, PDX, SRP058414, and TCGA). The factor explaining the greatest amount of variation in the data as plotted against the top eigenvectors is the source of data (i.e., batch effects).

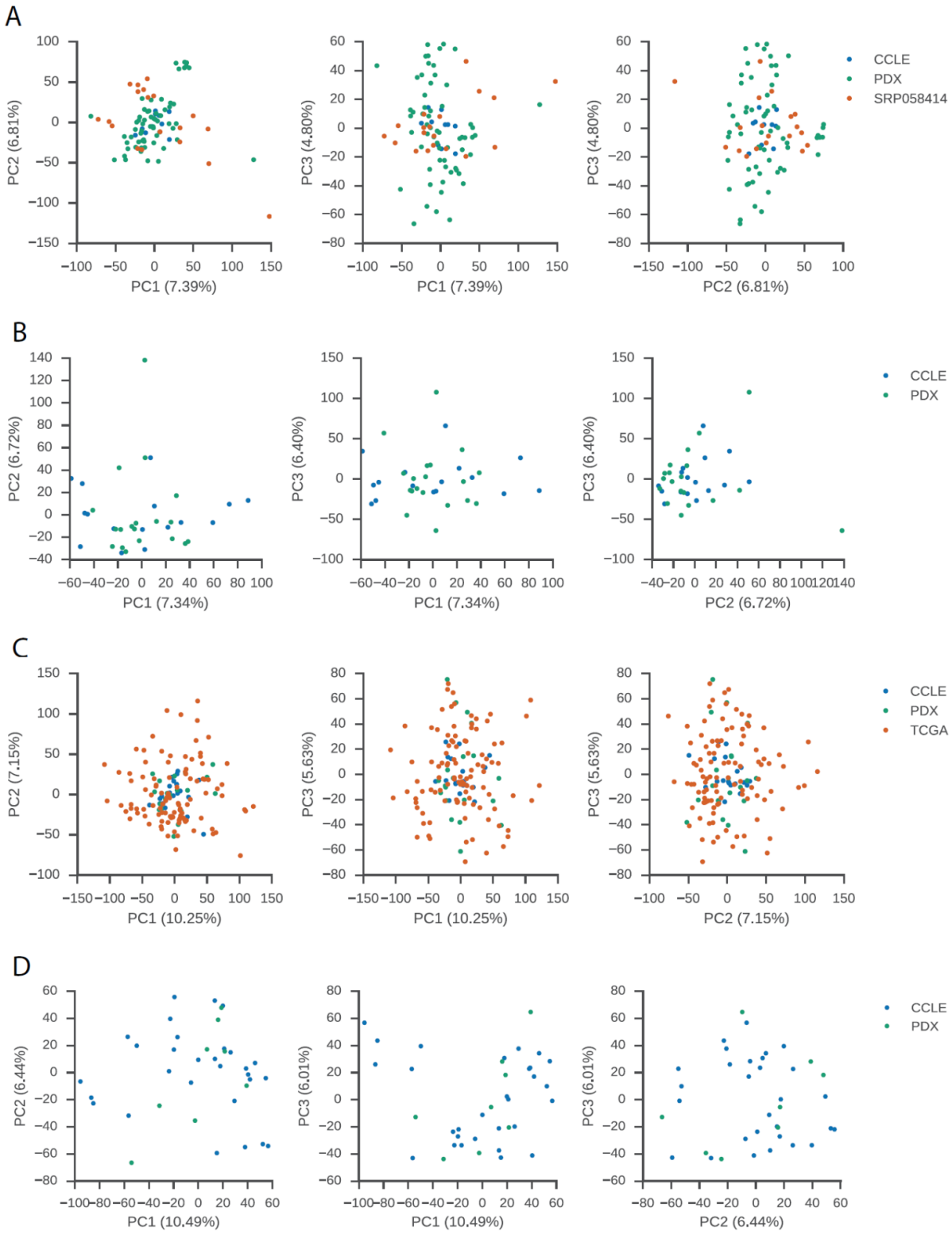
A
PC2 (6.81%)
PC1 (7.39%)
PC3 (4.80%)
PC1 (7.39%)
PC3 (4.80%)
PC2 (6.81%)
CCLE
PDX
SRP058414
B
PC2 (6.72%)
PC1 (7.34%)
PC3 (6.40%)
PC1 (7.34%)
PC3 (6.40%)
PC2 (6.72%)
CCLE
PDX
C
PC2 (7.15%)
PC1 (10.25%)
PC3 (5.63%)
PC1 (10.25%)
PC3 (5.63%)
PC2 (7.15%)
CCLE
PDX
TCGA
D
PC2 (6.44%)
PC1 (10.49%)
PC3 (6.01%)
PC1 (10.49%)
PC3 (6.01%)
PC2 (6.44%)
CCLE
PDX

Shown above is batch effect correction for normalized gene expressions from multiple data sets, as performed separately for each primary tumor histology using the ComBat approach from SVA 3.18.0 (A – B-ALL, B – T-ALL, C-AML, D-Lymphoma). Hierarchical clustering with Ward's linkage and Euclidean distance over the 750 genes with highest variance-to-mean ratio was performed separately for each histology (with external datasets) and over all histologies (only PDX samples). Fusion genes were called with STAR-Fusion 0.4.0 (https://star-fusion.github.io). Evidence for fusions was measured by summing spanning fragments (read pairs that align on both sides of a breakpoint) and junction reads (reads that align over the breakpoint). Fusions with an evidence of at least 10 over all samples were retained, and further filtered manually to conservatively remove putative homology induced artifacts.

Hemoseq

We analyzed the full coding sequences of a panel of 183 genes selected based on the presence of recurrent mutations in leukemia and lymphoma (Odejide et al., 2014; see **Table S2** for gene panel) in 115 PDX lines. Briefly, genomic DNA was extracted from banked xenografted tumor cells harvested from P0 (B-ALL) or ≥P1 mice (all other histologies) following immunomagnetic depletion of murine cells (EasySep Mouse/Human Chimera Isolation Kit, #19849, StemCell Technologies, Vancouver, BC, Canada). DNA underwent customized hybrid-capture target enrichment (SureSelect, Agilent, Santa Clara, CA, USA) and Illumina sequencing, as previously described (Odejide et al., 2014). Non-tumor DNA from remission peripheral blood, remission bone marrow, or saliva samples was also sequenced to exclude germ-line polymorphisms and platform-specific artifacts. Matched non-tumor samples were obtained from 45 of the 115 patients whose tumor-derived PDX lines were sequenced so as to facilitate filtering of somatic mutations. A panel-of-normals filter was subsequently generated from all 45 matched non-tumor controls. In addition, genomic DNA from the splenocytes of a normal NSG mouse was sequenced in order to enhance species-specific filtering of human reads. Sequencing reads were filtered using the NSG control and either the matched non-tumor sample, if available, or the panel-of-normals. Variants were rejected as germline artifacts if they were present in the matched non-tumor sample, if available; otherwise, they were rejected if present in two or more of the panel of normals. Known germline polymorphisms from the Exome Sequencing Project and the dbSNP (build 142) databases were also excluded. We applied the MutSigCV algorithm (Lawrence et al., 2013) to identify genes that were altered more often than expected by chance given the background mutation rate. We used the evolutionary conservation of the affected amino acid in protein homologues to predict the functional effect of detected variants. We only considered variants predicted to be non-silent (i.e., missense, nonsense, translational start site, or splice site alterations, or in-frame or frame-shift insertions/deletions) and with variant allele frequencies of 5% or more. For every alteration meeting these criteria, sequencing reads were individually visualized to evaluate mapping quality as well as the phase and spatial distribution of alterations within reads. Mutations were then called by cross-referencing candidate variants to ClinVar, COSMIC, and a review of published literature.

cDNA Production

For cDNA synthesis, cDNA was generated using the SuperScript III kit (Life Technologies) according to manufacturers directions. *TP53* cDNA was amplified using KOD Xtreme™ (EMD Millipore) with the following primers: *TP53*-f CATGGAGGAGCCGCAGTCAGA and *TP53*-r TCAGTCTGAGTCAGGCCCTTCTGTC and purified by PCR purification (Qiagen).

NanoString

All samples were assessed for quality and concentration using Agilent Bioanlayzer 2100. Capture, Reporter, and Plus product probes were hybridized to 100ng of total RNA at 65 deg C for 16hrs. Samples were washed and loaded onto a cartridge using the nCounter Analysis System Prep Station per the manufacturer's recommendations. The cartridge was scanned using the nCounter Digital Analyzer at the maximum resolution of 1150 FOV. One outlier from the NanoString analysis was the $TP53^{mut}$/CGM097-resistant sample, 88178, designated (d) in **Figure 4**. This sample demonstrated no CGM097-dependent gene expression in PD samples or the moribund-vehicle treated sample. However, expression of CGM097 was unexpectedly elevated in the CGM097-treated moribund sample. It is unclear how a sample with no CGM097-dependent gene expression at the PD time point would gain the activity over time. It is also unclear how a sample with a *TP53* mutation would demonstrateCGM097-dependent gene expression in any setting. However, western blotting demonstrated the expected pattern of elevated p53 expression with no p21 expression in both vehicle- and CGM097-treated moribund samples. Unlike all other PDXs, the data from the western blot is dissimilar to the data from Nanostring. This suggests that the sample analyzed by Nanostring may be different due to experimenter error.

FACS-based dynamic BH3 profiling

Dynamic BH3 profiling was performed as previously described (Montero et al., 2015; Pan et al., 2014; Ryan and Letai, 2013; Ryan et al., 2010). Briefly, B-ALL PDXs cells were incubated for 16 hours with 2μM CGM097 or DMSO in RPMI; then were pelleted at 500xg for 5 minutes, and resupsended in 100 μL PBS stained with 1μL per 10^6 cells of Live/Dead staining (Zombie Aqua dye, Biolegend) 20 min on ice. Cells were again pelleted at 500xg for 5 minutes, washed with PBS and resuspended in 100 μL 2% BSA/HBSS with human CD45 antibody (BD Horizon, BV421 clone HI30) 1:50 dilution, and human CD19 antibody (BDPharmingen PECy7 clone SJ25C1) 1:50 dilution for 30 minutes on ice, washed with PBS, and resuspended in DTEB buffer (Ryan et al., 2010) at a density of $1x10^6$ cells/mL. 25 μL of cell suspension was added to each well containing 25 μL of DTEB buffer containing 20 μg/mL Digitonin and peptides at twice their final concentration. Cells were incubated at room temperature for 60 minutes before terminating the exposure with 50 μL of 4% formaldehyde in PBS for 15 minutes at room temperature. Formaldehyde was then neutralized with 50 μL of N2 Buffer (1.7 M Tris, 1.25M glycine, pH 9.1) for 15 minutes at room temperature. To stain for retained cytochrome C, anti-cytochrome C clone 6H2.B4 conjugated to Alexafluor 488 (BD Bioscience) was diluted 1:50 into 10X stain buffer (1% Saponin, 10%BSA, 20%FBS in PBS) and 20 μL of this antibody/stain mixture was added to each well for a final antibody dilution of 1:360. Cells were stained overnight at 4°C and flow cytometry data acquired using a BD FACS Canto II.

Histology and Immunohistochemistry

Human specimens were fixed in 10% neutral-buffered formalin or B-plus fixative for up to 24 hours before paraffin embedding. Mouse PDX specimens were fixed in 10% neutral-buffered formalin for 48 hours and stored in 70% ethanol for up to 2 weeks before paraffin embedding. Immunohistochemical studies were performed on 4 micron paraffin sections using the following antibodies: CD3 (1:300; clone LN10, Leica Biosystems, Buffalo Grove, IL), CD20 (1:500; clone L26, Dako, Carpenteria, CA), PD-1 (1:100; clone NAT105, Cell Marque, Rocklin, CA), CD19 (1:150; clone BT51E, Leica), CD10 (1:80; clone 56C6, Leica), CD30 (1:75; clone Ber-H2, Dako), CD4 (1:100; clone EPR6855, Epitomics, Burlingame, CA), CD7 (1:100; clone CD7-272, Leica), CD8 (1:200; clone C8/144B, Dako), CD5 (1:400; clone 4C7, Leica), BCL2 (1:200; clone 124, Dako), TdT (1:100; clone SEN28, Leica), cyclin D1 (1:30; clone EPR2241, Thermo Scientific), PAX5 (1:100; clone 610863, BD, Franklin Lakes, NJ), and CD56 (1:50; clone 123C3, Dako). In situ hybridization for Epstein-Barr virus encoded RNA (EBER) was performed using the Ventana system (Tucson, AZ).

Clonality

Eight five-micron sections of formalin-fixed tissue were cut from paraffin blocks of each sample. The slides were scraped and DNA was isolated using the QIAamp DNA Mini Kit (QIAGEN, Valencia, CA). Human T-cell receptor gamma gene and immunoglobulin heavy chain gene rearrangement evaluation was performed per the BIOMED-2 protocol (van Dongen JJM et al. Leukemia. 2003, 17(12):2257-2317).

Supplemental References

Dobin, A., Davis, C.A., Schlesinger, F., Drenkow, J., Zaleski, C., Jha, S., Batut, P., Chaisson, M., and Gingeras, T.R. (2013). STAR: ultrafast universal RNA-seq aligner. Bioinformatics *29*, 15-21.

Grimwade, D., Hills, R.K., Moorman, A.V., Walker, H., Chatters, S., Goldstone, A.H., Wheatley, K., Harrison, C.J., Burnett, A.K., and National Cancer Research Institute Adult Leukaemia Working, G. (2010). Refinement of cytogenetic classification in acute myeloid leukemia: determination of prognostic significance of rare recurring chromosomal abnormalities among 5876 younger adult patients treated in the United Kingdom Medical Research Council trials. Blood *116*, 354-365.

Lawrence, M.S., Stojanov, P., Polak, P., Kryukov, G.V., Cibulskis, K., Sivachenko, A., Carter, S.L., Stewart, C., Mermel, C.H., Roberts, S.A.*, et al.* (2013). Mutational heterogeneity in cancer and the search for new cancer-associated genes. Nature *499*, 214-218.

Pan, R., Hogdal, L.J., Benito, J.M., Bucci, D., Han, L., Borthakur, G., Cortes, J., DeAngelo, D.J., Debose, L., Mu, H.*, et al.* (2014). Selective BCL-2 inhibition by ABT-199 causes on-target cell death in acute myeloid leukemia. Cancer Discov *4*, 362-375.

Ryan, J., and Letai, A. (2013). BH3 profiling in whole cells by fluorimeter or FACS. Methods *61*, 156-164.
Ryan, J.A., Brunelle, J.K., and Letai, A. (2010). Heightened mitochondrial priming is the basis for apoptotic hypersensitivity of CD4+ CD8+ thymocytes. Proceedings of the National Academy of Sciences of the United States of America *107*, 12895-12900.

Trapnell, C., Williams, B.A., Pertea, G., Mortazavi, A., Kwan, G., van Baren, M.J., Salzberg, S.L., Wold, B.J., and Pachter, L. (2010). Transcript assembly and quantification by RNA-Seq reveals unannotated transcripts and isoform switching during cell differentiation. Nat Biotechnol *28*, 511-515.